https://doi.org/10.5194/essd-2022-224
Preprint. Discussion started: 8 August 2022

Open Access Earth System Science Data Discussions

CALC-2020: a new baseline land cover map at 10 m resolution for the circumpolar Arctic

Chong Liu[1,2], Xiaoqing Xu[3], Xuejie Feng[1], Xiao Cheng[1,2], Caixia Liu[4], Huabing Huang[1,2]

[1]School of Geospatial Engineering and Science, Sun Yat-Sen University, Guangzhou, 510275, China
[2]Southern Marine Science and Engineering Guangdong Laboratory (Zhuhai), Zhuhai, 519000, China
[3]Peng Cheng Laboratory, Shenzhen, 518066, China
[4]Aerospace Information Research Institute, Chinese Academy of Sciences, Beijing, 100101, China

Correspondence to: Caixia Liu (liucx@radi.ac.cn) and Huabing Huang (huanghb55@mail.sysu.edu.cn)

Abstract. The entire Arctic is rapidly warming, which brings in a multitude of environmental consequences far beyond the northern high-latitude limits. Land cover maps offer biophysical insights into the terrestrial environment and are therefore essential for understanding the transforming Arctic in the context of anthropogenic activity and climate change. Satellite remote sensing has revolutionized our ability to capture land cover information over large areas. However, circumpolar Arctic-scale fine resolution land cover mapping has been so far lacking. Here, we utilize a combination of multimode satellite observations and topographic data at 10 m resolution to provide a new baseline land cover product (CALC-2020) across the entire terrestrial Arctic for circa 2020. Accuracy assessments suggest that the CALC-2020 product exhibits satisfactory performances, with overall accuracies of 79.63% and 67.27%, respectively, at validation sample locations and field/flux tower sites. The derived land cover map also displays reasonable agreement with three pre-existing global products, meanwhile depicting much more subtle polar biome patterns. Based on the CALC-2020 dataset, we show that over half of the Arctic landmass is covered by graminoid tundra or lichen/moss. Spatially, the land cover distribution exhibits regional dominance, reflecting the complex suite of both biotic and abiotic processes that jointly determine the Arctic landscape. The CALC-2020 product we developed can be used to improve earth system modelling, and benefit the ongoing efforts on sustainable Arctic land management by public and non-governmental sectors. The CALC-2020 land cover product is freely available on Science Data Bank: http://cstr.cn/31253.11.sciencedb.01869 (Xu et al., 2022a).

1 Introduction

Accounting for ~5.5% of the Earth's land surface, the Arctic disproportionately affects global biogeochemical cycles (Jeong et al., 2018; Landrum and Holland, 2020; Miner et al., 2022) and harbours a large proportion of high-latitude biodiversity (Niittynen et al. 2018; Christensen et al. 2020). During the past decades, the Arctic as a whole is rapidly warming (Previdi et al. 2021), with crucial consequences in the terrestrial section including land ice retreat (Shepherd et al., 2020), permafrost thawing (Hjort et al., 2018), vegetation greening/browning (Myers-Smith et al., 2020; Berner et al., 2020; Bartsch et al., 2020a), and intensified greenhouse gas emissions (Najafi et al. 2015). These changes have profound impacts on Arctic biomes

https://doi.org/10.5194/essd-2022-224
Preprint. Discussion started: 8 August 2022

(Hodkinson et al., 1998; Shevtsova et al., 2020; Wang and Friedl, 2019), as well as put millions of local residents and their cultures at risk (Huntington et al., 2019). Moreover, a changing Arctic is increasingly influencing human societies outside of the Arctic (Moon et al., 2019), through effects of sea level rise and atmospheric circulation. Without effective strategies for mitigating Arctic environmental changes, the goal of global sustainable development remains elusive (Beamish et al., 2020; Liu et al., 2021a, 2022).

As a key terrestrial surface descriptor, land cover is central to our understanding of the changing Arctic (Bartsch et al., 2016; Liang et al., 2019; Raynolds et al., 2019; Wang et al., 2020). The composition and distribution of land cover regulate the surface energy fluxes, which contribute to climate change and, in turn, influence land surface properties and the provision of ecosystem services (Friedl et al., 2010; Gong et al., 2013; Wulder et al., 2018; Song et al., 2018). Given the Arctic's ecological importance, some earlier studies have made attempts to map Arctic land cover based on field investigations (Ingeman-Nielsen and Vakulenko, 2018; Lu et al., 2018) or existing atlases (Walker et al., 2005; Raynolds et al., 2014), both of which are nevertheless laborious, time consuming and resource demanding. With synoptic view and repeatable coverage, satellite observations provide an unprecedented way to delineate and analyse Arctic land cover at multiple scales. However, previous remote sensing-based studies focused mainly on small areas (Kumpula et al., 2011; Yu et al., 2015; Jin et al., 2017; Wang et al., 2020), being unable to provide spatially complete information for the entire terrestrial Arctic. Some global land cover products may be used to overcome such difficulty (Hjort et al., 2018; Liang et al., 2019), but their strength is limited by the over simplification of classification schemes (Bartsch et al., 2016). For example, the widely used MODIS MCD12Q1 product only contains 2~3 classification types covering the whole Arctic landmass, making the characterization of heterogeneous biome pattern less feasible.

The recent advances in satellite data accessibility offers a new possibility to explore global environmental change (Gong et al., 2013; Brown et al., 2022). Rather than traditional land cover products derived from coarse-resolution imagery (e.g., the AVHRR-based IGBP DISCover map by Loveland et al. (2000)), now fine-resolution (10~30 m pixel size) remote sensing data are commonly utilized for capturing subtle patterns of biophysical composition, especially at continental to global scales (Li et al., 2019; Liu et al., 2020a; Zhang et al., 2020). Notwithstanding recent progress in land surface monitoring from space, circumpolar Arctic fine-resolution land cover mapping studies have been so far limited due to several factors. In the terrestrial Arctic, the common presence of small landscape patches gives rise to the "spectral confusion" issue that can lead to a decreased classification accuracy (Liang et al., 2019; Bartsch et al., 2020b). Moreover, cloud contamination and high solar zenith angles further introduce uncertainties into the results derived from optical imagery (Berner et al., 2020). In this regard, efforts of high-latitude land cover mapping should be complemented by information beyond the spectral domain. Space-borne Synthetic Aperture Radar (SAR) is capable of penetrating clouds and thus providing valuable earth observation information when and where valid optical image data are not available (Engram et al., 2013; Bartsch et al., 2020a; Bartsch et al., 2020b). In addition, a number of recent researches reported the potential of overcoming the obstacles in land cover mapping by incorporating terrain information (Zhu et al., 2016; Liu et al., 2018). Although promising, challenges in ground truth sample acquisition

https://doi.org/10.5194/essd-2022-224
Preprint. Discussion started: 8 August 2022


Open Access Earth System Science Data Discussions

hinder the practicability of multi-source remote sensing in the Arctic (Xu et al., 2022b), and there is still room for improvement regarding algorithm effectiveness and efficiency given the large satellite data volumes (Liu et al., 2020b, 2021c).

In this study, we present a new circumpolar Arctic land cover product for circa 2020 (CALC-2020 hereafter) through synergistically integrating multimode remote sensing data captured by the Sentinel satellite sensors and terrain layers derived from recently-released ArcticDEM. Within the Arctic extent, each land pixel is characterized by its dominant biophysical component using a modified FROM-GLC classification scheme, at 10 m spatial resolution. To create the CALC-2020 map, multiple metrics were derived from Sentinel-1 polarisation, Sentinel-2 surface reflectance and ArcticDEM topographic bands, serving as input features for a machine-learning classification procedure based on the Google Earth Engine (GEE) (Gorelick et al., 2017) platform. The classification model was locally calibrated with a training sample set migrated from the world's first all-season sample library and existing land cover products. We aim, by resolving the most updated spatial patterns and composition of land cover across the Arctic, to advance our knowledge of environmental change at northern high latitudes, and to enlighten sustainable land management by public and non-governmental sectors.

2 Materials and methods

2.1 Study area and classification scheme

It should be noted that there exist a number of definitions of what extent is contained within the Arctic. In the present study, we delimited the study area in the terrestrial Arctic, following our previous practices by Liu et al. (2021a) and Xu et al. (2022b). Here the terrestrial Arctic is defined as the northernmost part of the Earth characterized by tundra vegetation, an arctic climate and arctic flora, with the tree line and continental coastlines jointly determining the extent borders (**Figure 1**). Spatially, the present study covers an area of approximately 7.11 million km^2, overlapping with parts of six countries including Canada (CA), Denmark (Greenland, GR), Iceland (IC), Norway (NO), Russia (RU), and the United States (Alaska, AK). Within the study area, we implemented a ten-category classification scheme to represent the land cover diversity across the terrestrial Arctic. This scheme evolved from the level-1 classification system of FROM-GLC (Finer Resolution Observation and Monitoring of Global Land Cover) version 2017 (Gong et al., 2019), with necessary modifications that adapt to the geographical environment at northern high latitudes. More specifically, we excluded the grassland class due to its rareness, and subdivided the tundra biome into three categories: graminoid tundra, shrub tundra, and lichen/moss. **Table 1** provides the definition of each land cover type included in the present work.

https://doi.org/10.5194/essd-2022-224
Preprint. Discussion started: 8 August 2022

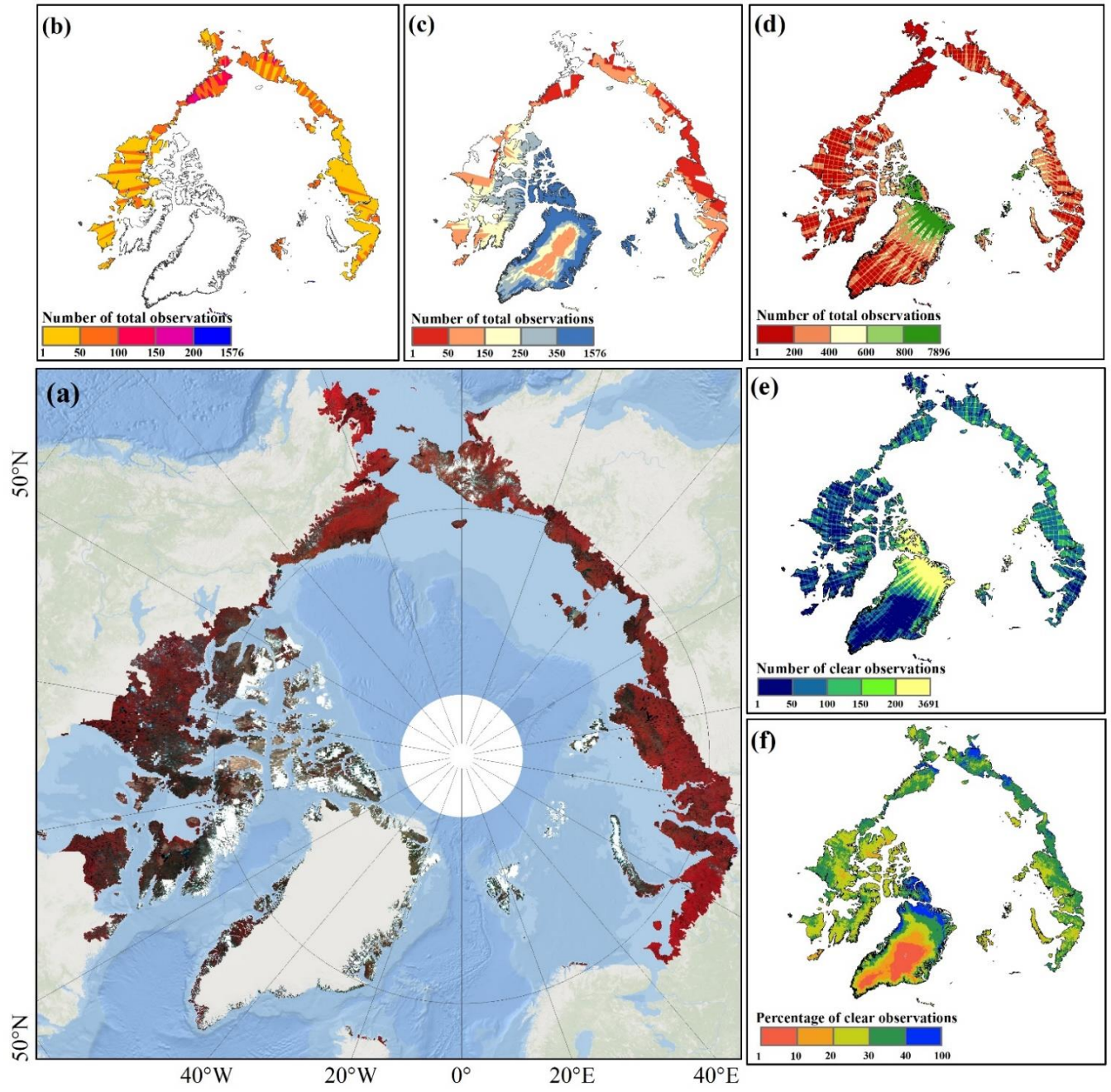

Figure 1: Overview of the study area. (a) Spatial extent of the circumpolar Arctic, located at the northernmost part of the Earth with a total area of ~7.11 million km^2. Bands 8, 4, 3 are displayed in as red, green and blue layers for the Sentinel-2 composite image. The base map is from ESRI. (b)~(c) show spatial distributions of per-pixel satellite observation availability for Sentinel-1 with VV+VH and HH+HV band combinations, respectively. (d)~(f) are spatial distributions of total observations, clear observations, and clear observation percentage of Sentinel-2.

https://doi.org/10.5194/essd-2022-224
Preprint. Discussion started: 8 August 2022

Table 1: Description of the ten-category land cover classification scheme used in the present work.

Land cover type (ID)	Description
Cropland (CRO)	Arable land that is sowed or planted at least once within a 12-month period, including irrigated or rain-fed field, plantation, and greenhouse
Forest (FST)	Land covered by trees, with canopy coverage greater than 30% and canopy height typically no less than 2 m
Graminoid tundra (GRT)	Land covered by herbaceous vegetations with plant height typically ranging 5~15 cm
Shrub tundra (SRT)	Land covered by shrubs of any stature (short or tall) with plant height typically ranging 20~50 cm
Wetland (WET)	Land featured by aquatic plants and periodically saturated with or covered by water
Open water (OWT)	Inland open water bodies, including rivers, lakes, reservoirs, pits and ponds
Lichen/moss (LAM)	Bedrock covered by cryptogam communities
Man-made impervious (MMI)	Impermeable land surface paved by man-made structures
Barren (BAR)	Natural dry land with vegetation coverage typically less than 10%
Ice/snow (IAS)	Land covered with snow and ice all year round

2.2 CALC-2020 input data

We used the GEE platform to obtain and preprocess remote sensing datasets in the present study. All image collections were independently filtered by the extent of the study area and the study period (the year 2020). The Sentinel-1 mission is composed of a constellation of two satellites (S-1A and S-1B), both performing dual-polarization C-band SAR imaging with a 12-day repeat cycle at the equator. Among various Sentinel-1 products, we used the Level 1 Ground Range Detected (GRD) product in the Interferometric Wide (IW) swath mode at 10 m spatial resolution. Given the imbalanced data coverage of polarization combinations across the Arctic (**Figure 1b~c**), we selected dual-band cross-polarization, horizontal transmit/vertical receive bands (HH+HV) for Canada and Greenland, and selected the dual-band cross-polarization, vertical transmit/horizontal receive bands (VV+VH) for the remaining countries. The Sentinel-2 Multi-Spectral Instrument (MSI) onboard both S-2A and S-2B satellites is an optical sensor having started observing the earth's terrestrial surface since 2015, with a spatial resolution of 10 to 60 m depending on the wavelength. The present study used the Level 2 surface reflectance product of Sentinel-2 to ensure that geometric and radiometric qualities meet the requirements. For each Sentinel-2 image, three visible bands, four red edge bands, three infrared bands and one quality assessment band (QA60) were employed. We pan-sharpened the red edge and infrared bands to 10 m using the bicubic interpolation algorithm (Liu et al., 2020a) to match the resolution of visible bands. In addition to satellite imagery, we also included the 10 m ArcticDEM digital surface model product in our data pool for

https://doi.org/10.5194/essd-2022-224
Preprint. Discussion started: 8 August 2022

characterizing the topographic properties of each pixel. Encompassing all land area north of 60°N, the ArcticDEM v3.0 product was generated from very high resolution (VHR) stereo images (Porter et al., 2018).

2.3 Creation of CALC-2020 map

Based on input data from Sentinel-1, Sentinel-2 and ArcticDEM, we developed a comprehensive framework (**Figure 2**) to guide circumpolar Arctic land cover mapping and analysis at 10 m spatial resolution for circa 2020. For the purpose of supervised classification model training and validation, a "ready for use" reference sample set was constructed based on the world's first all-season sample set (FAST) (Li et al., 2017). We created two separate circumpolar Arctic map products: a map of the man-made impervious surface extent and a map of the natural land cover distribution. For mapping the man-made impervious surface extent, we directly leverage the existing Circumpolar Arctic Man-made impervious area product (CAMI-2020) from our pilot study (Xu et al., 2022b). For mapping the natural land cover distribution, we constructed local adaptive random forest models for each country and performed supervised classification using polarimetric, spectral, phenological and topographic feature metrics. Detailed procedures within the framework are described below.

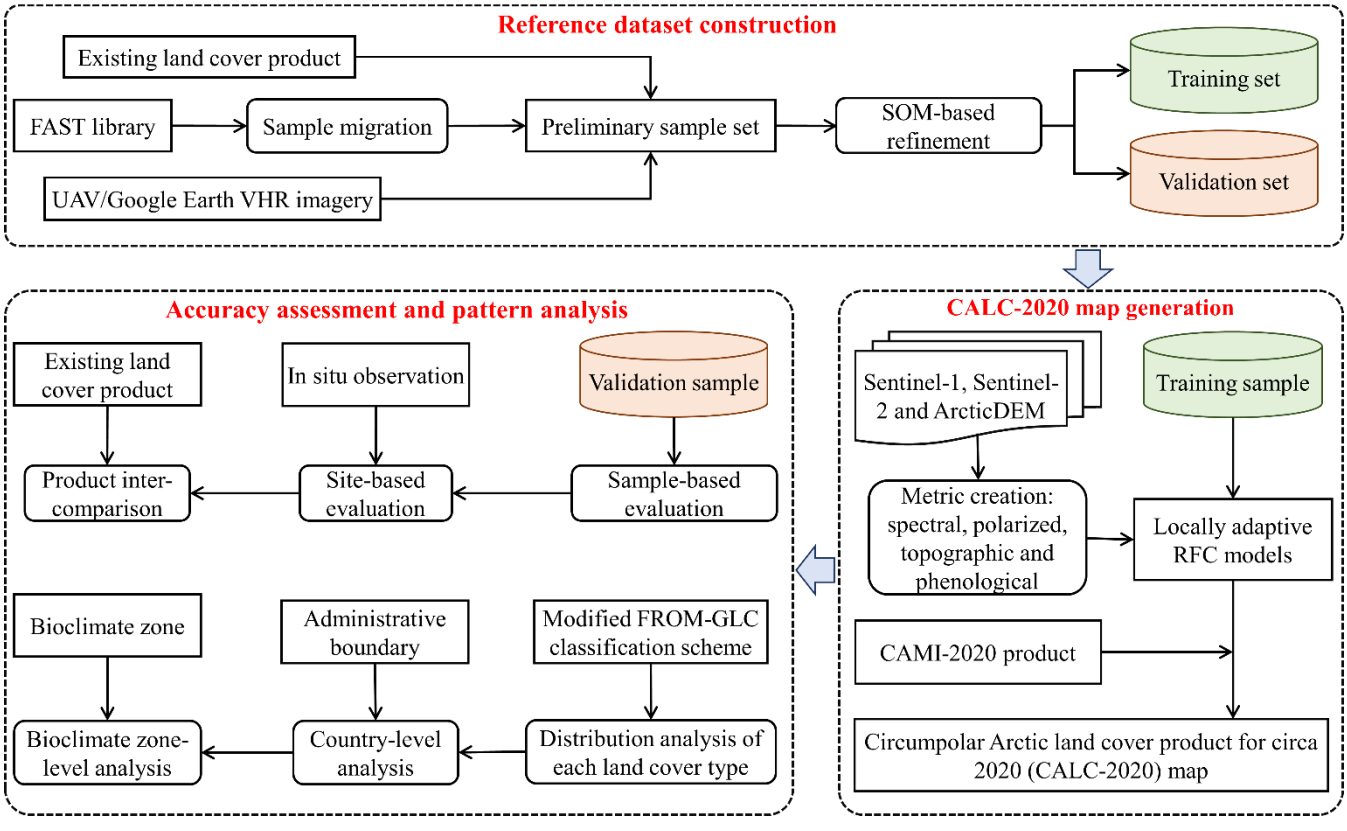

Figure 2: Framework of creating CALC-2020 map with the use of Sentinel-1, Sentinel-2 and ArcticDEM data.

https://doi.org/10.5194/essd-2022-224
Preprint. Discussion started: 8 August 2022

2.4.1 Construction of reference sample set

The supervised land cover classification approach requires reliable reference sample data for both model development and validation (Foody et al., 2016; Hermosilla et al., 2022). In the present study, a two-stage procedure was implemented to construct a reference sample set that is adequate and representative of intra-class variability over the terrestrial Arctic. At the first stage, we used the recently released FAST sample library to generate the backbone of a preliminary sample set. FAST offers over 90,000 sample locations and their multi-seasonal land cover type information at the planetary scale (Li et al., 2017). We followed the sample migration approach by Huang et al. (2020) to remove FAST records that experienced land cover changes. Moreover, for each FAST sample record within our study area, a 90×90 m buffer was created for homogeneity check, and only sample locations exhibiting the same land cover types with their surrounding areas were preserved. Besides the migrated FAST data, we additionally extracted sample records from three existing land cover maps, including NLCD 2016 (for Alaska), Land Cover of Canada 2015 (for Canadian Arctic), and GlobeLand30 V2020 (for the rest terrestrial Arctic countries). For each used land cover product, a stratified random sampling strategy was employed to balance both rare and common classes (Zhu et al., 2016). It should be noted that neither FAST nor pre-existing land cover products contains the lichen/moss class, which requires special consideration. In the present study, lichen/moss sample records were derived from visual interpretation using the Google Earth VHR imagery data as primary reference. Available UAV aerial images provided by the United States Geological Survey (USGS) were also used to refine the judgements.

Due to classification scheme inconsistence and acquisition year mismatch among multiple reference datasets, the preliminary sample set inevitably contains errors that could undermine or even lead to the failure of CALC-2020 mapping. Therefore, at the second stage, we conducted a refinement approach to obtain a "ready for use" sample set based on the self-organizing map (SOM) technique. The SOM, also known as Kohonen neural network, is an effective and automatic tool for the task of clustering and classification (Kohonen, 2013). It represents the input data distribution by using a two-dimensional map in which models are automatically associated with neurons. In this study, we created and trained a 10×10 map of 100 neurons using the batch Weight/Bias training algorithm implemented in MATLAB R2016a. The map training completes when the maximum number of epochs (i=200) reached. **Figure 3** illustrates the procedure of SOM-based sample refinement. For a given a land cover class C (other land cover classes termed Rs), we randomly selected N sample records labelled as C and $2N$ sample records labelled as Rs, respectively, from the preliminary sample set. These two sample subsets were merged and feature metrics were derived for each sample position **(see 2.4.3)**. We then used the SOM algorithm to group the merged sample set into 100 clusters, within each of which the purity index was acquired by calculating the percentage of sample records labelled as C. We only kept clusters with the purity index values greater than 75%. This approach was applied to all classes for constituting the "ready for use" sample set. After the SOM-based refinement, the final reference sample set includes 84,410 valid records, with their circumpolar Arctic distribution shown in **Figure S1**. We randomly split the final reference sample set into two independent parts: 80% (70,260 sample records) for training the classification models and the other 20% (14,150 sample records) for accuracy assessment.

https://doi.org/10.5194/essd-2022-224
Preprint. Discussion started: 8 August 2022

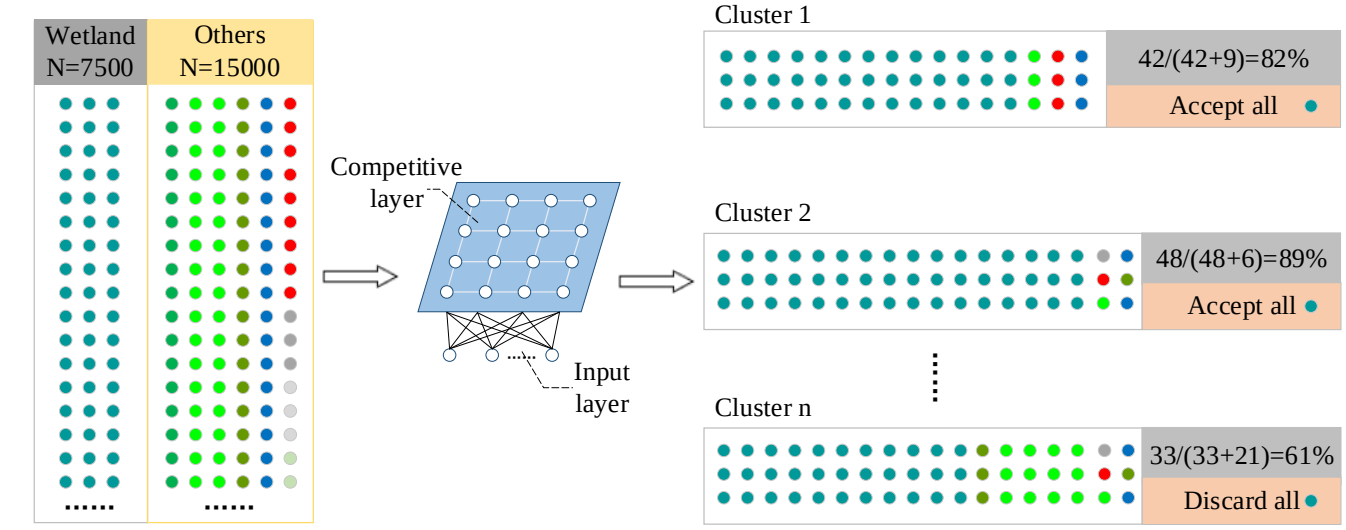

Figure 3: Illustration of the SOM-based sample refinement procedure.

2.4.2 Man-made impervious surface mapping

Man-made impervious surface is a representative land cover type indicating human footprint. However, mapping man-made impervious surface has been difficult because it consists of diverse artificial materials and spatial forms (Li and Gong, 2016). This issue becomes more prominent in the Arctic where impervious surface clusters are usually fragmented and small in size (e.g. oil/gas deposits). Therefore, we leveraged the existing product, CAMI-2020, from our pilot study (Xu et al., 2022b) to pre-classify Arctic man-made impervious surfaces. CAMI-2020 was developed by integrating satellite imagery and OpenStreetMap as input features; it provides the first spatially continuous map of Arctic man-made impervious surface distribution at 10 m resolution. Accuracy assessment suggests that the CAMI-2020 map is capable of capturing the spatial patterns of man-made impervious surface across the Arctic, with overall accuracy and Kappa value of 86.4% and 0.7, respectively. Due to its robustness, CAMI-2020 can be used for delimiting the Arctic man-made impervious surface extent in the present study. The CAMI-2020 dataset is publicly available from http://www.doi.org/10.11922/sciencedb.01435.

2.4.3 Natural land surface mapping

Multiple feature metrics derived from Sentinel-1, Sentinel-2 and ArcticDEM were employed to facilitate the natural surface land cover mapping. For Sentinel-1, a seasonal compositing approach was undertaken to obtain the median value of all valid observations for growing months (June, July, and August) and dormant months, separately. For Sentinel-2, three groups of feature metrics were employed over the study year: (i) per-band values representing growing season reflectance using median and greenest compositing methods, respectively; (ii) per-index values representing selected percentiles (10%, 50% and 90%);

https://doi.org/10.5194/essd-2022-224
Preprint. Discussion started: 8 August 2022

(iii) phenometrics including the start of growing season (SOS), end of growing season (EOS), the peak of growing season (POS), and the largest data value of growing season (LDOG). We followed the algorithm of Bolton et al. (2020) to estimate the phenometrics. Cloud-free Sentinel-2 observations were first interpolated in each pixel at an 8-day time step using penalized cubic smoothing splines. Then the normalized difference vegetation index (NDVI) was calculated at each temporal interval to depict the time (day of year, DOY hereafter) of the vegetation phenophase transitions. The maximum value of the smoothed NDVI time series was identified as LDOG. SOS and EOS were retrieved as the DOYs when the NDVI time series cross 50% of the amplitude in the greenup and greendown periods, respectively. POS was identified as the DOY when the NDVI time series reaches LDOG. Topographic metrics were computed from ArcticDEM, including elevation, slope, and aspect. In summary, we created 51 feature metrics for natural land surface classification. **Table S1** provides a summary of the metrics used in the present study.

Based on all metric sets described above, we used Random Forest Classifier (RFC) to generate Arctic's natural land cover map. RFC is a non-parametric machine learning method that ensembles a multitude of decision trees for class membership prediction (Breiman, 2001). Compared with other supervised classification algorithms, RFC is more robust in mapping large-area land cover and can accommodate high dimension input features (Zhu et al., 2012; Gong et al., 2020a; Zhang et al., 2021a). For the purpose of balancing classification accuracy and computational efficiency, we parameterized RFC with 500 decision trees and the square root of the total number of input variables as the number of variables to split each node (Liu et al., 2019). RFC model training and prediction were performed individually for each country using the "smileRandomForest" API in GEE.

2.5 Mapping performance evaluation

The evaluation for the land cover classification was conducted in three ways. First, we used the established validation sample set to assess the accuracy of our CALC-2020 map. For each of the Arctic countries, we obtained the confusion matrix and calculated quantitative metrics including overall accuracy (OA), the Kappa coefficient, producer's accuracy (PA) and user's accuracy (UA). To further verify the balance of commission and omission errors, we also calculated the minimum accuracy (MA), which is defined as the minimum of PA and UA for all classes (Zhu et al., 2016). In the second validation method, we evaluated the CALC-2020 mapping performance using in situ data obtained from ORNL DAAC's MODIS/VIIRS Land Product Subsets project (ORNL DAAC 2018). We employed the Fixed Sites Subsets Tool to select all field and flux tower sites within our study area (55 sites in total, **Table S2**). For each site, the dominant land cover type was determined by referring to its meta data as well as the near-surface camera images (if available). In the third validation method, we inter-compared our mapping results with three global land cover products: the ESA WorldCover V100 (Zanaga et al., 2020), the ESRI Global Land Cover (Karra et al., 2021), and the GlobeLand30 V2020 (Chen et al., 2015). There products were selected because they have consistent data epoch and adequate spatial resolutions that make them directly comparable to CALC-2020 map. Comparison of CALC-2020 with other three land cover products was implemented both statistically and spatially to understand the overestimation or underestimation of each land cover type.

https://doi.org/10.5194/essd-2022-224
Preprint. Discussion started: 8 August 2022

3 Results and discussion

3.1 Reliability of CALC-2020 map

3.1.1 Sample-based evaluation

Table 2 shows sample-based accuracy summary statistics of the CALC-2020 map per study country and the Arctic as a whole. In general, the OA and Kappa evaluated against independent reference sample are 79.63% and 0.76, respectively. Spatially, we found the land cover classifications of all study countries have satisfactory accuracies, with OA ranging from 73.47% (Canada) to 84.61% (Russia). Similarly, most study countries exhibit reasonable Kappa coefficients (above 0.7), except for Alaska and Canada with a slightly less desirable result (0.67). In addition, a rather wide MA range (from 47.67% to 64.38%) is observed among six Arctic countries. The largest MA level stands out in Russia (64.38%), followed by Greenland and Alaska with over 55% of MA values. The lowest MA level occurs in Canada, where more than half of the graminoid tundra validation sample points are misclassified as other land cover types.

We further evaluated the CALC-2020 map for different land cover types by calculating their PA and UA metrics. As shown in Figure 4, the CALC-2020 product provides reliable mapping results across different Arctic geographical environments. There are five classes (forest, graminoid tundra, lichen/moss, barren and permanent snow/ice) showing higher PA accuracies than UA accuracies, suggesting a tendency of high commission errors for these land cover types. On the contrary, for cropland, shrub tundra, wetland, open water and man-made impervious surface, accuracies measured by PA are slightly lower than those by UA, suggesting a tendency of high omission error. This accuracy assessment by class reflects an overall balanced estimation by our classification result. By disaggregating PA and UA metrics into the country level, we were able to quantify spatial differences in mapping performance among biomes. Referring to PA, the largest inter-country discrepancy exists in the Shrub tundra. In contrast, the wetland exhibits a greater UA variation than other land cover classes.

Table 2: Country-specific classification accuracy of the CALC-2020 map. AK, CA, IC, GR, NO and RU represent Alaska, Canada, Iceland, Greenland, Norway and Russia, respectively. OA indicates overall accuracy, and MA indicates minimum accuracy with the corresponding land cover type shown in the parentheses. Land cover abbreviations are given in Table 1.

	Overall	AK	CA	IC	GR	NO	RU
OA (%)	79.63	75.71	73.47	77.82	80.35	78.94	84.61
MA (%)	58.29 (LAM)	55.07 (WET)	47.67 (GRT)	50.77 (BAR)	55.66 (BAR)	52.42 (LAM)	64.38 (BAR)
Kappa	0.76	0.67	0.67	0.74	0.76	0.75	0.81
Number of sample unit	14150	2856	3860	779	1878	870	3907

https://doi.org/10.5194/essd-2022-224
Preprint. Discussion started: 8 August 2022

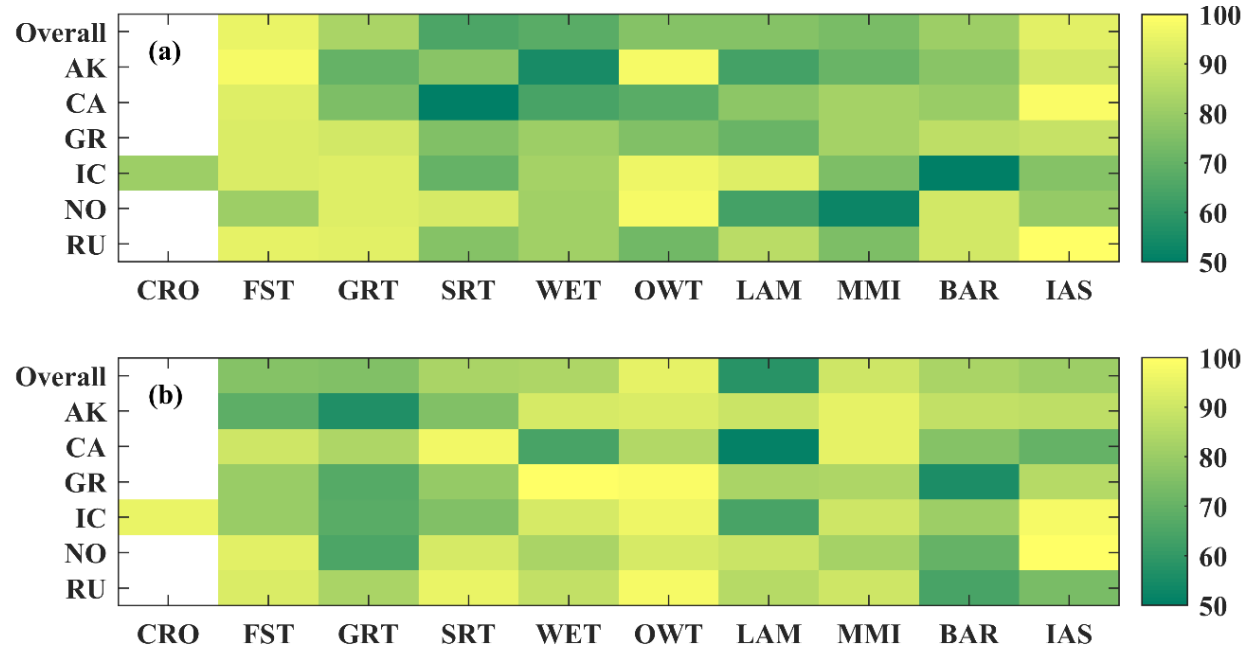

Figure 4: Accuracy matrixes of the CALC-2020 map for each land cover type. Color scales in (a) and (b) represent the range of producer's accuracy (PA) and user's accuracy (UA), respectively. Land cover abbreviations are given in Table 1. It should be noted that croplands are only distributed in Iceland.

3.1.2 Land cover mapping performance in field and flux tower sites

Figure 5 displays the alluvial diagram of performance evaluation for the CALC-2020 product in field and flux tower sites. Overall, our satellite-derived land cover classification is reasonably consistent with the in situ reports. There are 37 out of 55 sites showing consistent classification results, with OA and Kappa value being equal to 67.27% and 0.56, respectively. When the analysis is broken down into the biome level, we found the biggest error source comes from confusion among different vegetation types. In particular, there are six wetland sites and three shrubland tundra sites that were mistakenly identified as graminoid tundra. These discrepancies reflect the complex suite of factors that can obscure the correct identification of Arctic biomes. For example, some wetland vegetation species are morphologically similar to gramineous plants, thus limiting the classification accuracy (Magnússon et al., 2021). The relatively poor mapping performance of Arctic vegetations could be also attributed to the short growing season (typically ranging from 50 to 60 days), in which satellite coverage is commonly spatially and temporally uneven (Beamish et al., 2020). Considerable misclassifications were also observed in some sites dominated by man-made impervious surfaces, suggesting the technical challenge of capturing small-scale artificial imperviousness using the CALC-2020 map. It is important to point out that the field and flux tower sites used in the present work are not evenly distributed over space and across biomes. Some land cover types (e.g., forest and lichen/moss) have very limited sites after data screening, making them less representative for mapping performance evaluation. This situation would be improved as more ground and near-surface reference data become available in the future (Richardson et al., 2018; Pastorello et al., 2020).

https://doi.org/10.5194/essd-2022-224
Preprint. Discussion started: 8 August 2022

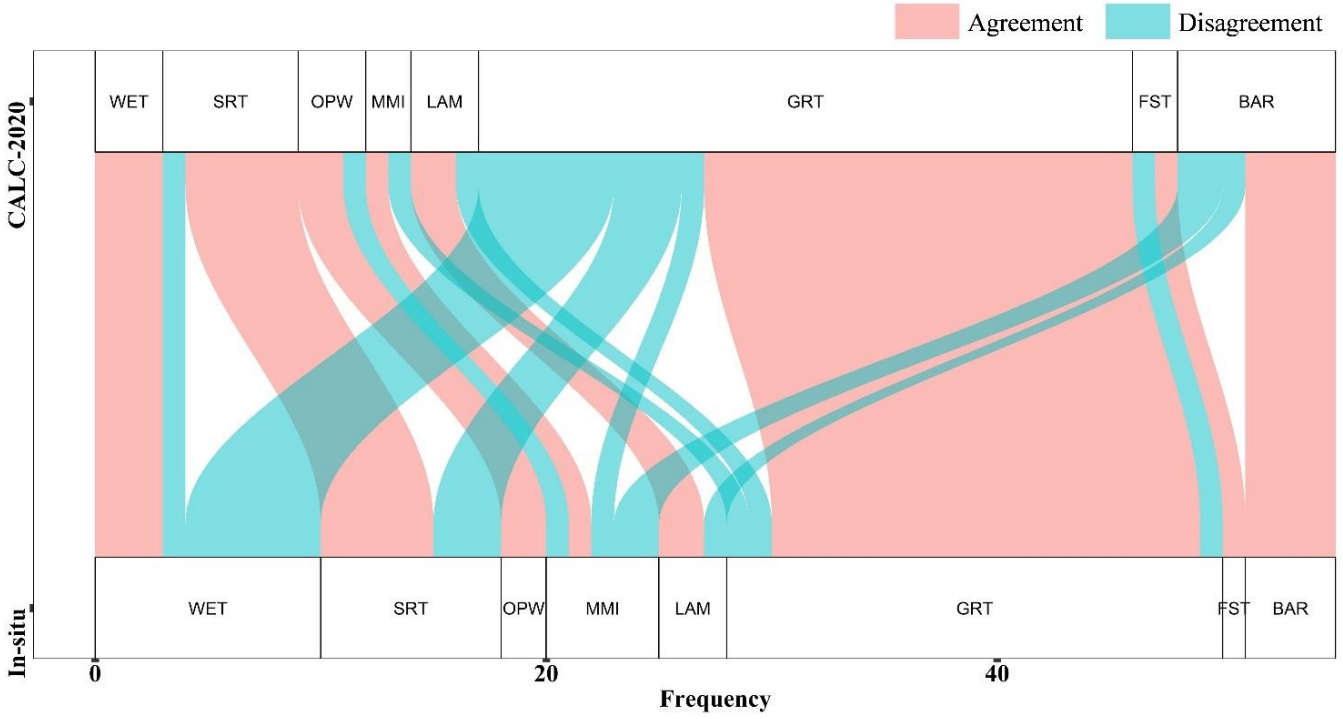

Figure 5: CALC-2020 map performance in 55 field and flux tower sites. The block width represents the frequency (site number) identified by our estimation and in situ reports, respectively. Land cover abbreviations are given in Table 1.

3.1.3 Comparison with existing land cover products

Figure 6 displays the spatial patterns and statistics of agreement/discrepancy between our CALC-2020 map and three existing land cover products by treating our estimates as the baseline. At the per-pixel level, the paired land cover comparison result consists of four categories: classification agreement (AG), classification disagreement due to model prediction (DM), classification disagreement due to scheme difference (DS), and classification disagreement due to data missing (DD). Overall, the mapped comparison outputs exhibit considerable variations at the circumpolar Arctic scale. Based on the statistics, the GlobeLand30 exhibits the largest area proportion of AG (45%), which is closely followed by the ESA WorldCover (41%). By contrast, the lowest agreement level occurs in the ESRI Global Land Cover map, where more than 70% of the valid pixels show discrepancies. The mapped disagreements were induced by multiple drivers. DS is the primary source of discrepancy between our estimation and ESRI Global Land Cover. The dominant role of DS was also commonly observed in Alaska and Russia, with the ESA WorldCover product used for comparison. DM, on the other hand, prevailed in all countries when comparing the CALC-2020 map to the GlobeLand30 dataset. Consistently across all country domains, DD plays a minor role with very limited area occupation. Within each country, the spatial patterns of the agreement level also vary substantially. For example, in Canadian Arctic, a latitudinal north (high)–south (low) contrast in land cover mapping agreement is evident.

https://doi.org/10.5194/essd-2022-224
Preprint. Discussion started: 8 August 2022

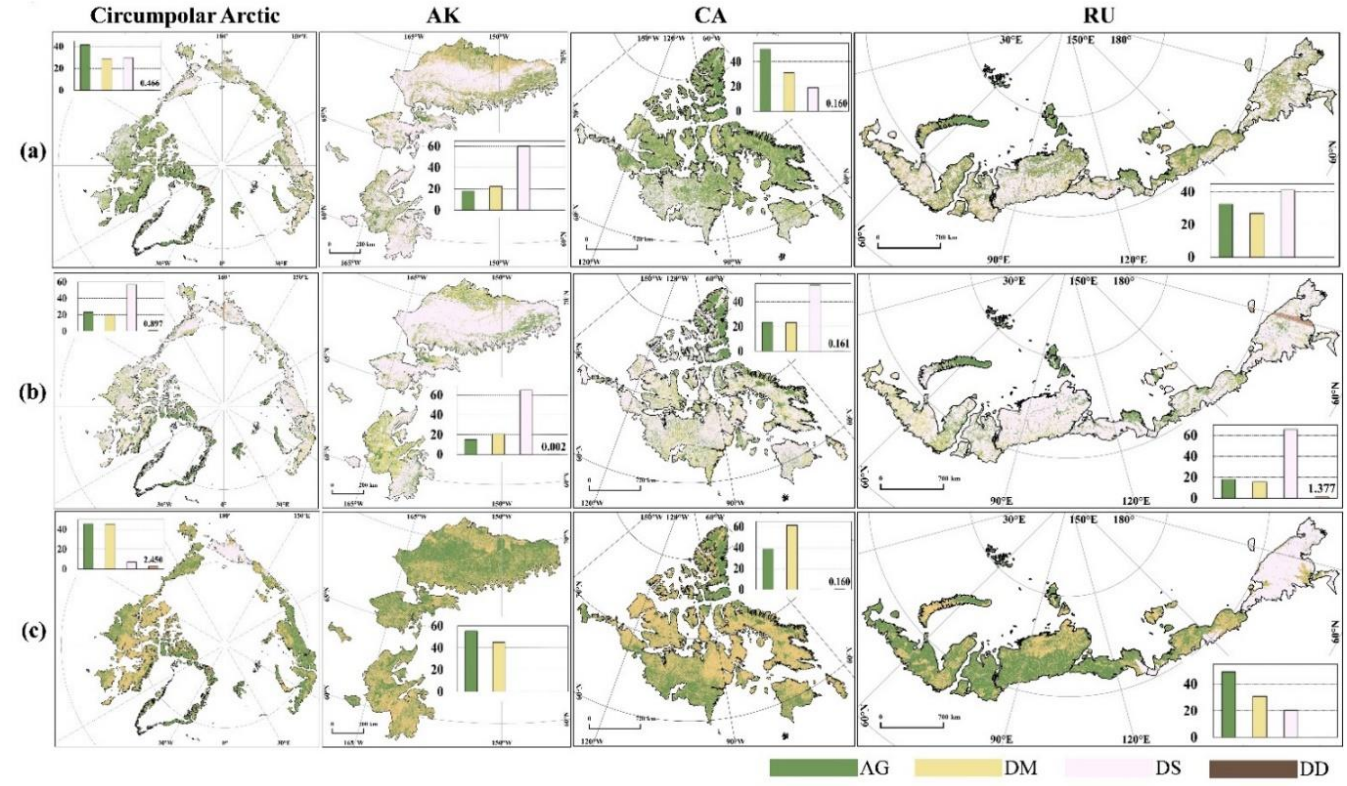

Figure 6: The spatial distributions of the classification consistency between the CALC-2020 estimation and three existing global land cover products including the ESA WorldCover V100 (a), the ESRI Global Land Cover (b), and the GlobeLand30 V2020 (c). The histogram in each panel shows the pixel frequency distributions of the four categories: classification agreement (AG), classification disagreement due to model prediction (DM), classification disagreement due to scheme difference (DS), and classification disagreement due to data missing (DD).

Figure 7 further compares multiple land cover datasets by selecting four sub-regions, each of which represents one typical landscape across the terrestrial Arctic. The land cover products are displayed with their corresponding classification schemes. In Keewatin (Canada), all the products correctly captured most open water areas. Compared to other datasets, our CALC-2020 map is more similar to GlobeLand30 in terms of the overall vegetation composition and distribution. In North Slope (Alaska), our estimate detects the coexistence of graminoid tundra and shrub tundra, with their distributions highly related to topographic characteristics. This heterogenous land cover pattern, however, is not observed in other three products. The largest mapping discrepancy is found in Yamal Peninsula (Russia), where more than half of the landmass is covered by thermokarst lakes. Our dataset is generally consistent with GlobeLand30, but providing much more spatial details. ESA WorldCover and ESRI Global Land Cover, on the other hand, show greater wetland estimates. Moreover, the CALC-2020 is the only product that fully depicts the distribution of man-made impervious surfaces (oil/gas deposits and traffic pavements). In Nenets (Russia), major forest clusters are identified by the three datasets with a finer resolution of 10 m, including CALC-2020, ESA WorldCover, and ESRI Global Land Cover). However, the latter two products are not able to isolate graminoid plants from wetlands, both of which are clearly displayed by our mapping result.

https://doi.org/10.5194/essd-2022-224
Preprint. Discussion started: 8 August 2022

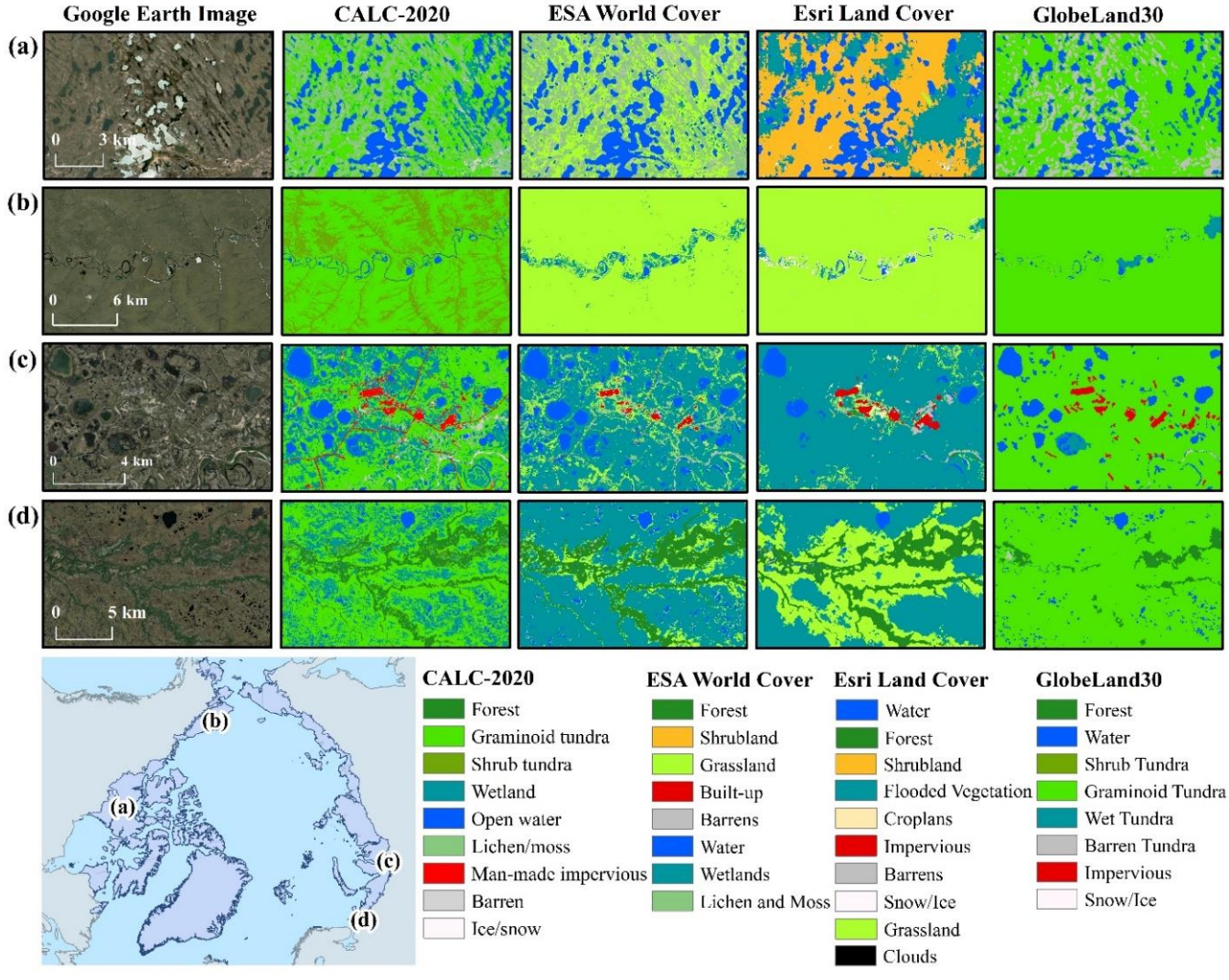

Figure 7: Comparison of CALC-2020 mapping results with other land cover products in four typical sub-regions. (a) Keewatin in Canada, centred at 65.3°N, 99.1°W. (b) North Slope in Alaska, centred at 69. 5°N, 156.0°W. (c) Yamal Peninsula in Russia, centred at 67.9°N, 75.5°E. (d) Nenets in Russia, centred at 66.6°N, 47.2°E. © Google Earth.

3.2 Spatial patterns and composition of circumpolar Arctic land cover

The CALC-2020 product provides the first spatially continuous map of circumpolar Arctic land cover at 10 m resolution (**Figure 8a**). Based on this map, we calculated the distribution densities of all land cover types at the 1°×1° tile scale (**Figure 8b~k**), as well as their total area statistics throughout the terrestrial Arctic (**Figure 8l**). Among all land cover classes, the graminoid tundra occupies the largest Arctic land area (1709,530 km^2, 28.92%), closely followed by the lichen/moss class (1394,130 km^2, 23.58%). In contrast, croplands and man-made impervious surfaces play a very minor role with limited area occupation (less than 1,000 km^2). There also exist differences in spatial patterns across land cover classes. For example,

https://doi.org/10.5194/essd-2022-224
Preprint. Discussion started: 8 August 2022

clustered hotspots of forest and shrub tundra are only found in Alaska and Southern Nenets in Russia. Stress-tolerant biomes (i.e., graminoid tundra and lichen/moss), on the other hand, occupy the most parts of the terrestrial Arctic, although the latter exhibits a northward distribution shift. For Arctic wetlands, a latitudinal north (less)–south (more) contrast in fractional coverage is evident, which closely corresponds to the distribution of open water areas. Conversely, barren and ice/snow
305 coverages are more frequently detected in middle to high Arctic regions, such as Greenland, Svalbard archipelago, and Canadian Arctic Archipelago. Our map also provides observational evidence of human action on Arctic landscapes, primarily via man-made imperviousness encroachment. This is the result of persistent disturbances from industrial infrastructure development and traffic pavement (Bartsch et al., 2021; Xu et al., 2022b).

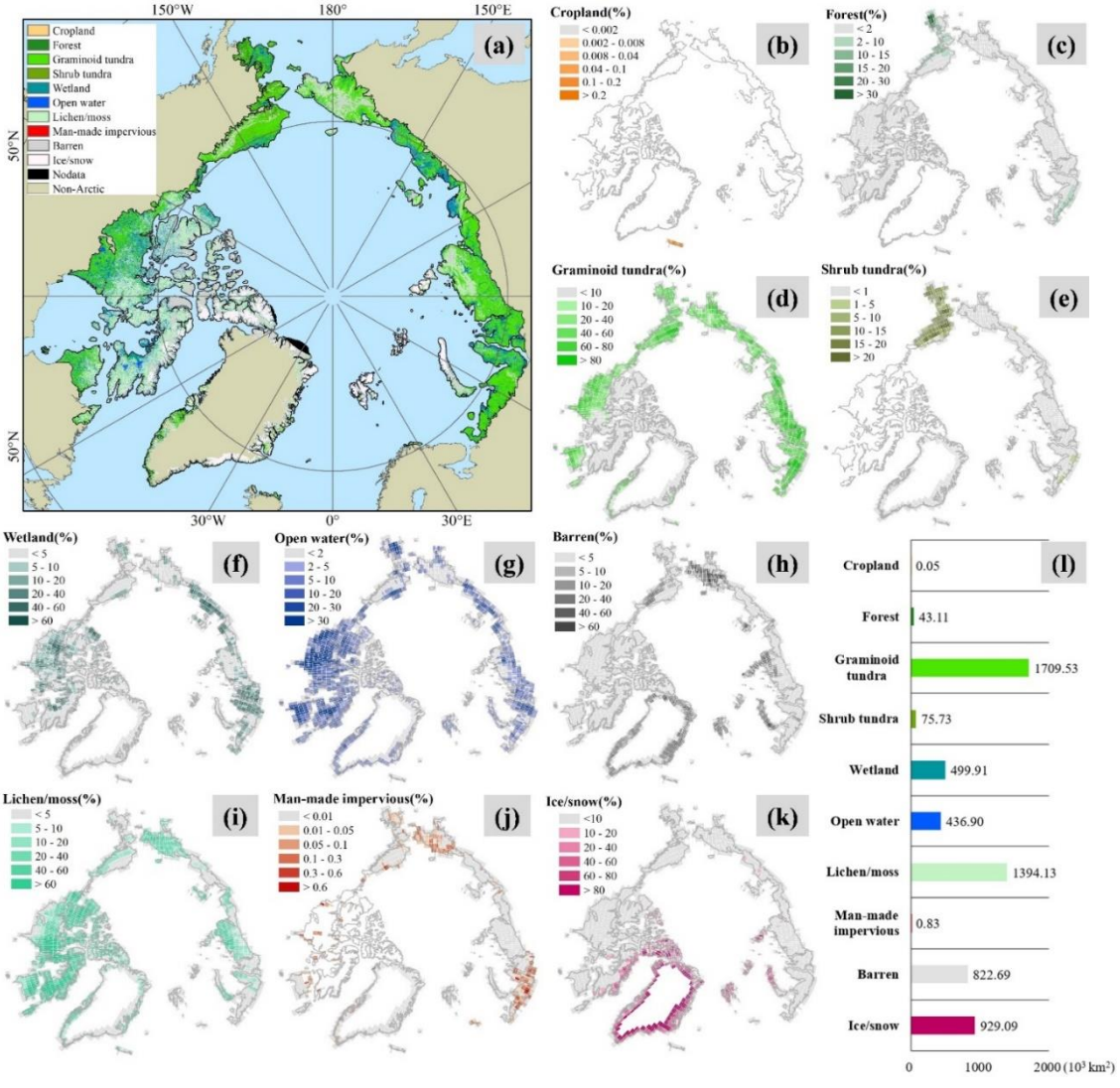

310 **Figure 8: Circumpolar Arctic land cover estimated by the CALC-2020 map. (a) Land cover distribution at the 10 m pixel scale. (b)~(k) display the biome-specific area proportion in each 1°×1° land tile. (l) shows area statistics of all land cover types across the terrestrial Arctic (unit of 10^3 km^2).**

https://doi.org/10.5194/essd-2022-224
Preprint. Discussion started: 8 August 2022

Land cover compositions are unevenly distributed across countries (**Figure 9a**). The largest area proportion of vegetated coverage occurs in Alaska (85.8%), which is comparable to Russia (80.4%). In contrast, Canada and three Nordic countries (Greenland, Iceland and Norway) contain more non-vegetated areas covered by open water bodies, bare lands and snow/ice grounds. Consistently among all countries, stress-tolerant biomes (graminoid tundra and lichen/moss) play a more prominent role than the other vegetation classes. In addition, Alaska is the only statistical unit with over 20% landmass occupied by woody plants (shrub tundra and forest). We further divided the entire terrestrial Arctic into five bioclimate zones defined by summer warmth index (SWI, the sum of monthly mean air temperatures greater than 0°C) (Jia et al., 2003), and found a transition in land cover composition as SWI gradually increases (**Figure 9b**). The overall area proportion loss in snow/ice and bare land mirrors vegetation cover gain, together confirming that warm conditions are generally optimal for Arctic plant growth (Keenan and Riley, 2018).

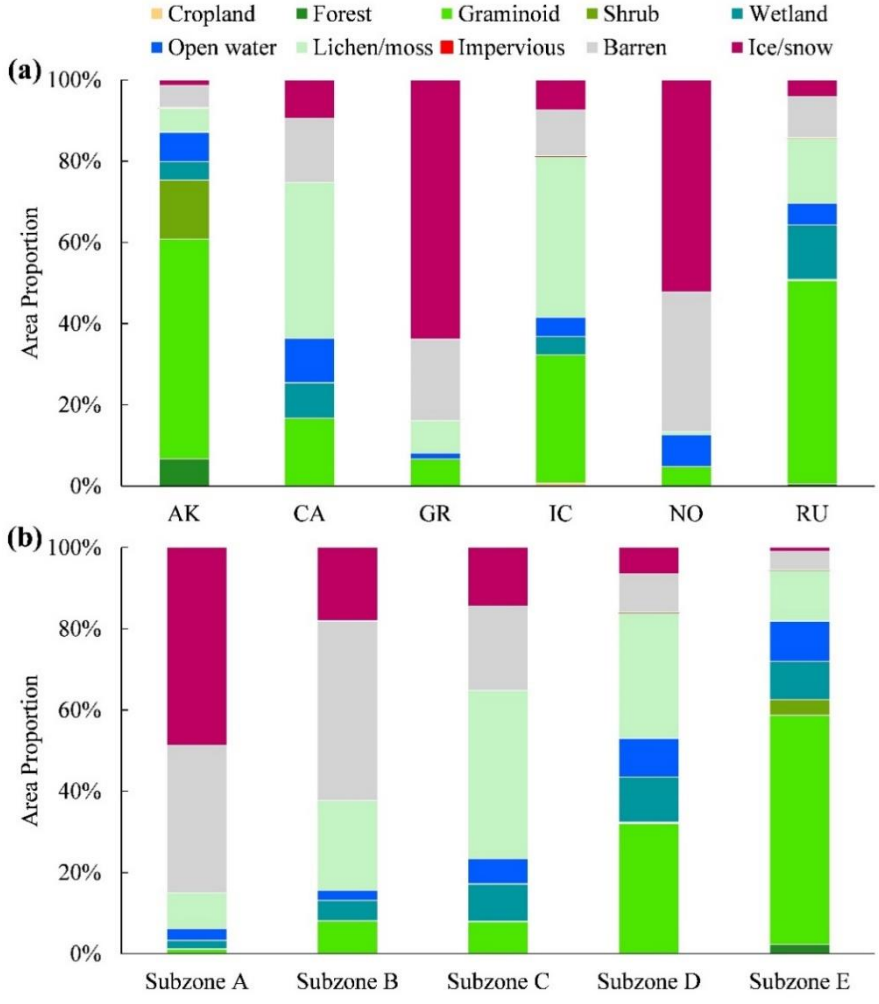

Figure 9: Circumpolar Arctic land cover composition calculated at country (a) and bioclimate zone (b) levels, respectively. Subzone A~E correspond to SWI sections (°C): <6, 6≤SWI<9, 9≤SWI<12, 12≤SWI<20, SWI≥20.

https://doi.org/10.5194/essd-2022-224
Preprint. Discussion started: 8 August 2022

3.3 Methodological and scientific implications

Fine resolution mapping of circumpolar Arctic land cover is a challenging task from almost every aspect of satellite remote sensing, including data acquisition, classification scheme design, feature extraction, and accuracy assessment. Our study highlighted the necessity of including both active and passive Earth observations to create a seamless land cover map across the entire terrestrial Arctic (Bartsch et al., 2016). We observed high cloud contamination (clear Sentinel-2 observation percentage less than 40%) in over half of the Arctic landmass (**Figure 2**), where Sentinel-1 SAR images can be useful to enhance the robustness of land cover type identification. The utilization of multi-source features is also beneficial for distinguishing land surface characteristics that are difficult to classify from the spectral domain alone. **Figure 30** displays the feature importance, quantified by total decrease in Gini impurity index over all trees in the RFC model. Consistently across all countries, topography is the most helpful feature domain, which is in line with previous studies and supports the idea that, at high latitudes of the Northern Hemisphere, the land cover distribution is subject to climate and terrain conditions (Walker et al., 2005; Jin et al., 2017). In addition, SAR features are more effective than spectral features for classification. Compared with original reflectance bands, spectral indices and phenological metrics are generally more important, although both of them may only have substantial impacts on certain land cover classes (Friedl et al., 2010; Huang et al., 2022).

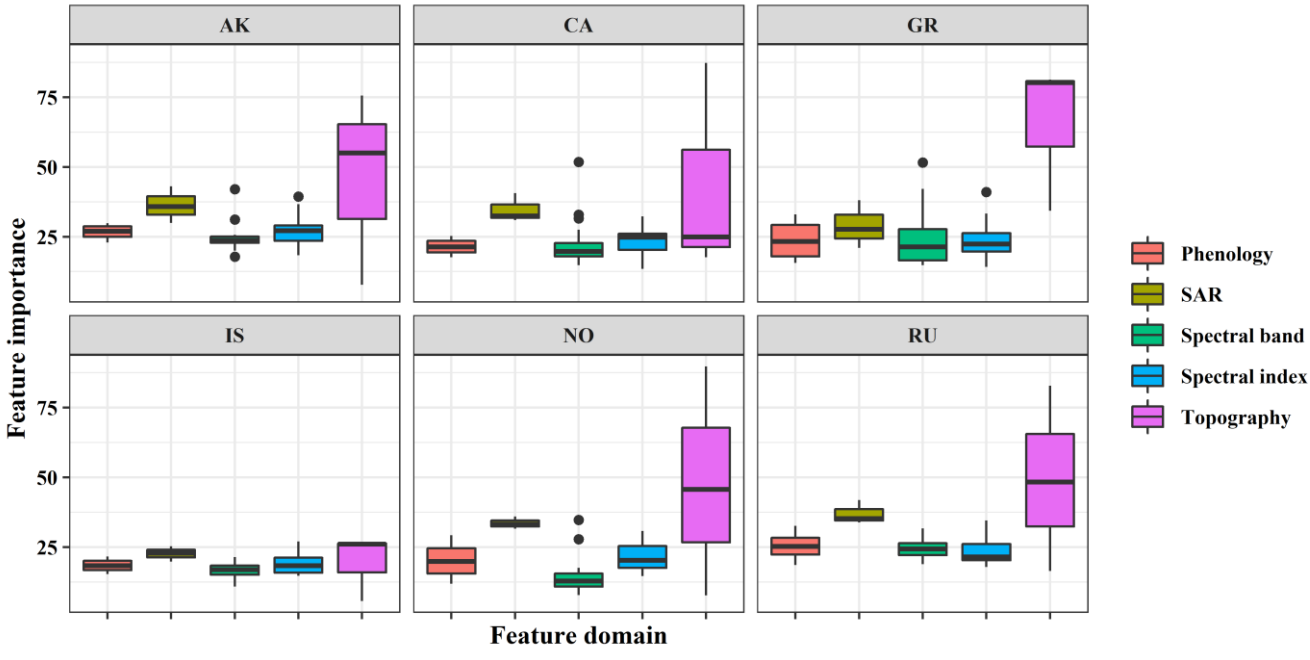

Figure 10: Box plots showing the contribution variation among different feature domains at the country level. The feature importance is measured by total decrease in Gini impurity index over all trees in the RFC model. Country abbreviations are given in Table 2.

https://doi.org/10.5194/essd-2022-224
Preprint. Discussion started: 8 August 2022

The land cover legend should reflect the information content of the study area to be interpreted (Wulder et al., 2018; Song et al., 2018; Zhang et al., 2021a). Currently, debate still exists on the determination of classification scheme system over the terrestrial Arctic (Bartsch et al., 2016). For example, the widely used IGBP classification system (Friedl et al., 2010; Loveland and Belward, 1997) contains 17 categories, but very few of them appear at the northern high latitudes (Liang et al., 2019). By contrast, some well-known polar biomes (e.g., lichen/moss) are absent in existing global land cover products (**Figure 7**), making the description of complex landscape over-simplified. In the present study, we designed a ten-category classification scheme that is generally consistent with the Circumpolar Arctic Vegetation Map (CAVM) (Walker et al., 2005; Raynolds et al., 2019), thus carrying the potential for discriminating Arctic plant communities with a fine spatial resolution. However, it is worth noting that some biomes exhibit very strong intra-class variability in physiognomy, which makes the proposed classification scheme less desirable. For example, a short shrubland tundra environment is a fundamentally different ecosystem from a tall one and this influences a vast array of biotic and abiotic processes (Walker et al., 2005). With updates of more multi-source Earth observation data (e.g., vegetation height (Lang et al., 2022)), building a hierarchical Arctic land cover class scheme is becoming a possible topic, which is worthy of exploration in the future.

Generating reliable training and validation data has always been a critical constraint on land cover mapping applications. Traditionally, reference sample data can be either collected from field surveys (Gong et al., 2020b) or interpreted from remotely sensed images (Liu et al., 2019; Brown et al., 2020; Potapov et al., 2022). These approaches, however, are laborious or even unrealistic in remote and inaccessible areas, such as the Arctic. Alternatively, several studies demonstrated the potential of deriving reference sample from pre-existing knowledge (Gray and Song, 2013; Hakkenberg et al., 2020). Building on this premise, our study takes a step forward by developing a "ready for use" sample set migrated from the FAST library for supervised classification model calibration and evaluation. Given the global coverage and sufficient sample size, our FAST-based sample migration strategy can be applied to various ecological zones, and particularly useful in ecoregions where land cover reference data are not available. In addition to the sample-based validation, we also evaluated the CALC-2020 product with other two assessment data sources: site records and contemporary global land cover products. With precisely known location and relatively homogeneous biome footprint, near-ground site networks (e.g., FLUXNET, PhenoCam) provide the most unbiased information for land cover mapping accuracy assessment (Gong, 2008). Unfortunately, these networks are currently sparse in the Arctic, and the site number of some land cover types is very limited (**Table S2**, **Figure 5**), making them less representative for Pan-Arctic applications. Comparing the CALC-2020 dataset with existing global land cover products is complementary to the sample/site analysis in characterizing pixel-level agreement, and we found varied levels of mapping consistence over space (**Figure 6~7**). In addition to the classification scheme mismatch issue mentioned above, another primary cause of the performance difference may be algorithm structure of identifying land cover types. Rather than directly adopting a universal predictive framework, the land cover class information in this study was derived from locally adaptive (country-specific) RFC models, so the unfavourable impacts incurred by geographical variability can be largely reduced (Zhang et al., 2021a; Huang et al., 2022).

https://doi.org/10.5194/essd-2022-224
Preprint. Discussion started: 8 August 2022

Arctic ecosystem function is highly dependent on land cover composition and distribution, yet both of them remain poorly understood (A'Campo et al., 2021; Wang and Friedl, 2019; Beamish et al., 2020). We expect that the CALC-2020 product will help fill the scientific gap by providing the most recent circumpolar biophysical conditions in the Northern Hemisphere. For example, accurate land cover data are key inputs for projecting biogeochemical cycles under current and future scenarios, thus guiding local, national, and global efforts of climate change mitigation (Horvath et al., 2021; Zhang et al., 2021b). Previous studies have found a poleward movement of the Arctic treeline—northernmost edge of the habitat where trees are capable of growing. Our estimation that circumpolar Arctic forest cover reaches approximately 43,000 km^2 suggests woody encroachment as the climate warms, and is thus consistent with the forest growth trend (Harsch et al., 2009; Rees et al., 2020). However, our results differ from previous studies by identifying the subtle distribution pattern of trees with a much finer spatial resolution (**Figure 11**). Finally, using the CALC-2020 product as the baseline, along with decades of satellite observation wealth, circumpolar land cover change monitoring can be possibly crafted, which will advance our understanding of a continuously changing Arctic and its global environmental impacts.

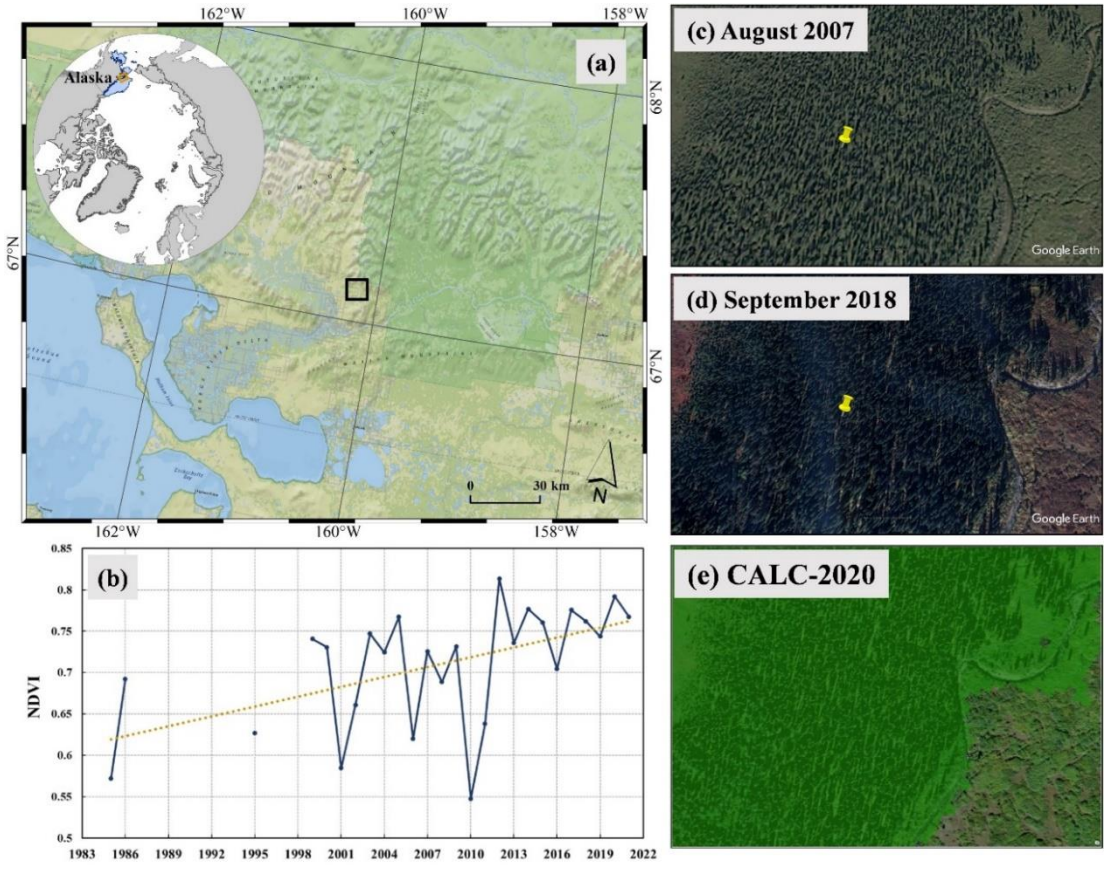

Figure 11: Satellite observed afforestation in the Arctic. (a) Location of afforestation centred at 67.1°N, 160.2°W; (b) annual median Landsat NDVI time series from 1984 to 2021; (c)~(d) comparison of two VHR images acquired in 2007 and 2018, respectively (© Google Earth); (e) forest extent derived from the CALC-2020 product. The topographic map was generated using ESRI basemap layer product.

https://doi.org/10.5194/essd-2022-224
Preprint. Discussion started: 8 August 2022

4 Data availability

The CALC-2020 product generated in this paper is available on Science Data Bank: http://cstr.cn/31253.11.sciencedb.01869 (Xu et al., 2022a). Across the entire Arctic, the CALC-2020 product consists of six files in GeoTIFF format with a 10 m spatial resolution (EPSG: 6931). Each land cover map file is named based on the following rule: "CALC-2020-X.tif". The "X" in the file name represents its mapping country (AK, CA, GR, IC, NO, RU). Country abbreviations are given in **Table 2**. The valid values for the land cover types are 0~10. The CALC-2020 product was generated on the GEE platform using the JavaScript language developed by the authors.

5 Conclusions

A thorough understanding of Arctic terrestrial changes requires information about both the composition and the distribution of land covers. In this study, we developed a circumpolar Arctic land cover product for circa 2020 using fine resolution multi-source remote sensing data. Based on a "ready for use" sample set migrated from FAST, the CALC-2020 map was generated through a locally adaptive machine-learning classification procedure. Accuracy assessments reveal the reliability of CALC-2020, as well as its representativeness for characterizing the Arctic ecosystem in ways that are not well represented by pre-existing products. According to our estimation, the graminoid tundra occupies the largest Arctic land area, and the latitudinal shift of land cover composition is generally consistent with the SWI gradient profile. Our mapping results also offer the evidence of woody encroachment, especially in Alaska and Southern Nenets, Russia. We concluded that the new CALC-2020 map can be used to augment the modelling of both biotic and abiotic processes, thus enlightening innovative Arctic management.

Author contributions

Chong Liu, Caixia Liu, and Huabing Huang carried out the analysis and wrote the manuscript; Xiaoqing Xu and Xuejie Feng helped with the data processing and the accuracy assessment; Xiao Cheng conceived the study. All authors helped revise the manuscript.

Competing interests

The authors declare that they have no conflict of interest.

https://doi.org/10.5194/essd-2022-224
Preprint. Discussion started: 8 August 2022

Financial support

The research was supported by the National Key R&D Program of China (2019YFC1509105, 2019YFC1509104), and Guangdong Natural Science Foundation (2022A1515010924).

Acknowledgments

The authors acknowledge the Google Earth Engine platform, which makes circumpolar Arctic-scale geospatial mapping and analysis possible at fine spatial resolutions. We are also grateful to all data providers that have been used in this study.

References

A'Campo, W., Bartsch, A., Roth, A., Wendleder, A., Martin, V. S., Durstewitz, L., Lodi, R., Wagner, J., and Hugelius, G.: Arctic Tundra Land Cover Classification on the Beaufort Coast Using the Kennaugh Element Framework on Dual-Polarimetric TerraSAR-X Imagery, Remote Sens., 13, https://doi.org/10.3390/rs13234780, 2021.

Bartsch, A., Höfler, A., Kroisleitner, C., and Trofaier, A. M.: Land Cover Mapping in Northern High Latitude Permafrost Regions with Satellite Data: Achievements and Remaining Challenges, Remote Sens., 8, https://doi.org/10.3390/rs8120979, 2016.

Bartsch, A., Widhalm, B., Leibman, M., Ermokhina, K., Kumpula, T., Skarin, A., Wilcox, E. J., Jones, B. M., Frost, G. V., Höfler, A., and Pointner, G.: Feasibility of tundra vegetation height retrieval from Sentinel-1 and Sentinel-2 data, Remote Sens. Environ., 237, 111515, https://doi.org/10.1016/j.rse.2019.111515, 2020a.

Bartsch, A., Pointner, G., Ingeman-Nielsen, T., and Lu, W.: Towards Circumpolar Mapping of Arctic Settlements and Infrastructure Based on Sentinel-1 and Sentinel-2, Remote Sens., 12, https://doi.org/10.3390/rs12152368, 2020b.

Bartsch, A., Pointner, G., Nitze, I., Efimova, A., Jakober, D., Ley, S., Högström, E., Grosse, G., and Schweitzer, P.: Expanding infrastructure and growing anthropogenic impacts along Arctic coasts, Environ. Res. Lett., 16, 115013, https://doi.org/10.1088/1748-9326/ac3176, 2021.

Beamish, A., Raynolds, M. K., Epstein, H., Frost, G. V., Macander, M. J., Bergstedt, H., Bartsch, A., Kruse, S., Miles, V., Tanis, C. M., Heim, B., Fuchs, M., Chabrillat, S., Shevtsova, I., Verdonen, M., and Wagner, J.: Recent trends and remaining challenges for optical remote sensing of Arctic tundra vegetation: A review and outlook, Remote Sens. Environ., 246, 111872, https://doi.org/10.1016/j.rse.2020.111872, 2020.

Berner, L. T., Massey, R., Jantz, P., Forbes, B. C., Macias-Fauria, M., Myers-Smith, I., Kumpula, T., Gauthier, G., Andreu-Hayles, L., Gaglioti, B. V., Burns, P., Zetterberg, P., D'Arrigo, R., and Goetz, S. J.: Summer warming explains widespread but not uniform greening in the Arctic tundra biome, Nat. Commun., 11, 4621, https://doi.org/10.1038/s41467-020-18479-5, 2020.

Bolton, D. K., Gray, J. M., Melaas, E. K., Moon, M., Eklundh, L., and Friedl, M. A.: Continental-scale land surface phenology from harmonized Landsat 8 and Sentinel-2 imagery, Remote Sens. Environ., 240, 111685, https://doi.org/10.1016/j.rse.2020.111685, 2020.

Breiman, L.: Random Forests, Mach. Learn., 45, 5–32, https://doi.org/10.1023/A:1010933404324, 2001.

https://doi.org/10.5194/essd-2022-224
Preprint. Discussion started: 8 August 2022

Brown, C. F., Brumby, S. P., Guzder-Williams, B., Birch, T., Hyde, S. B., Mazzariello, J., Czerwinski, W., Pasquarella, V. J., Haertel, R., Ilyushchenko, S., Schwehr, K., Weisse, M., Stolle, F., Hanson, C., Guinan, O., Moore, R., and Tait, A. M.: Dynamic World, Near real-time global 10 m land use land cover mapping, Sci. Data, 9, 251, https://doi.org/10.1038/s41597-022-01307-4, 2022.

Brown, J. F., Tollerud, H. J., Barber, C. P., Zhou, Q., Dwyer, J. L., Vogelmann, J. E., Loveland, T. R., Woodcock, C. E., Stehman, S. V., Zhu, Z., Pengra, B. W., Smith, K., Horton, J. A., Xian, G., Auch, R. F., Sohl, T. L., Sayler, K. L., Gallant, A. L., Zelenak, D., Reker, R. R., and Rover, J.: Lessons learned implementing an operational continuous United States national land change monitoring capability: The Land Change Monitoring, Assessment, and Projection (LCMAP) approach, Remote Sens. Environ., 238, 111356, https://doi.org/10.1016/j.rse.2019.111356, 2020.

Chen, J., Chen, J., Liao, A., Cao, X., Chen, L., Chen, X., He, C., Han, G., Peng, S., Lu, M., Zhang, W., Tong, X., and Mills, J.: Global land cover mapping at 30m resolution: A POK-based operational approach, ISPRS J. Photogramm. Remote Sens., 103, 7–27, https://doi.org/10.1016/j.isprsjprs.2014.09.002, 2015.

Christensen, T., Barry, T., Taylor, J. J., Doyle, M., Aronsson, M., Braa, J., Burns, C., Coon, C., Coulson, S., Cuyler, C., Falk, K., Heiðmarsson, S., Kulmala, P., Lawler, J., MacNearney, D., Ravolainen, V., Smith, P. A., Soloviev, M., and Schmidt, N. M.: Developing a circumpolar programme for the monitoring of Arctic terrestrial biodiversity, Ambio, 49, 655–665, https://doi.org/10.1007/s13280-019-01311-w, 2020.

Engram, M., Anthony, K. W., Meyer, F. J., and Grosse, G.: Synthetic aperture radar (SAR) backscatter response from methane ebullition bubbles trapped by thermokarst lake ice, Can. J. Remote Sens., 38, 667–682, https://doi.org/10.5589/m12-054, 2013.

Foody, G. M., Pal, M., Rocchini, D., Garzon-Lopez, C. X., and Bastin, L.: The Sensitivity of Mapping Methods to Reference Data Quality: Training Supervised Image Classifications with Imperfect Reference Data, ISPRS Int. J. Geo-Inf., 5, https://doi.org/10.3390/ijgi5110199, 2016.

Friedl, M. A., Sulla-Menashe, D., Tan, B., Schneider, A., Ramankutty, N., Sibley, A., and Huang, X.: MODIS Collection 5 global land cover: Algorithm refinements and characterization of new datasets, Remote Sens. Environ., 114, 168–182, https://doi.org/10.1016/j.rse.2009.08.016, 2010.

Gong, P.: Accuracies of global land cover maps checked against fluxnet sites, Sci. Found. China, 16, 2008.

Gong, P., Wang, J., Yu, L., Zhao, Y., Zhao, Y., Liang, L., Niu, Z., Huang, X., Fu, H., Liu, S., Li, C., Li, X., Fu, W., Liu, C., Xu, Y., Wang, X., Cheng, Q., Hu, L., Yao, W., Zhang, H., Zhu, P., Zhao, Z., Zhang, H., Zheng, Y., Ji, L., Zhang, Y., Chen, H., Yan, A., Guo, J., Yu, L., Wang, L., Liu, X., Shi, T., Zhu, M., Chen, Y., Yang, G., Tang, P., Xu, B., Giri, C., Clinton, N., Zhu, Z., Chen, J., and Chen, J.: Finer resolution observation and monitoring of global land cover: first mapping results with Landsat TM and ETM+ data, Int. J. Remote Sens., 34, 2607–2654, https://doi.org/10.1080/01431161.2012.748992, 2013.

Gong, P., Liu, H., Zhang, M., Li, C., Wang, J., Huang, H., Clinton, N., Ji, L., Li, W., Bai, Y., Chen, B., Xu, B., Zhu, Z., Yuan, C., Suen, H. P., Guo, J., Xu, N., Li, W., Zhao, Y., Yang, J., Yu, C., Wang, X., Fu, H., Yu, L., Dronova, I., Hui, F., Cheng, X., Shi, X., Xiao, F., Liu, Q., and Song, L.: Stable classification with limited sample: transferring a 30-m resolution sample set collected in 2015 to mapping 10-m resolution global land cover in 2017, Sci. Bull., 64, 370–373, https://doi.org/10.1016/j.scib.2019.03.002, 2019.

Gong, P., Li, X., Wang, J., Bai, Y., Chen, B., Hu, T., Liu, X., Xu, B., Yang, J., Zhang, W., and Zhou, Y.: Annual maps of global artificial impervious area (GAIA) between 1985 and 2018, Remote Sens. Environ., 236, 111510, https://doi.org/10.1016/j.rse.2019.111510, 2020a.

Gong, P., Chen, B., Li, X., Liu, H., Wang, J., Bai, Y., Chen, J., Chen, X., Fang, L., Feng, S., Feng, Y., Gong, Y., Gu, H., Huang, H., Huang, X., Jiao, H., Kang, Y., Lei, G., Li, A., Li, X., Li, X., Li, Y., Li, Z., Li, Z., Liu, C., Liu, C., Liu, M., Liu, S., Mao, W., Miao, C., Ni, H., Pan, Q., Qi, S., Ren, Z., Shan, Z., Shen, S., Shi, M., Song, Y., Su, M., Suen, H. P., Sun, B., Sun, F., Sun, J., Sun, L., Sun, W., Tian, T., Tong, X., Tseng, Y., Tu, Y., Wang, H., Wang, L., Wang, X., Wang, Z., Wu, T., Xie, Y., Yang, J., Yang, J., Yuan, M., Yue, W., Zeng, H., Zhang, K., Zhang, N., Zhang, T., Zhang, Y., Zhao, F., Zheng, Y., Zhou, Q., Clinton, N., Zhu, Z., and Xu, B.: Mapping essential urban land use categories in China (EULUC-China): preliminary results for 2018, Sci. Bull., 65, 182–187, https://doi.org/10.1016/j.scib.2019.12.007, 2020b.

Gorelick, N., Hancher, M., Dixon, M., Ilyushchenko, S., Thau, D., and Moore, R.: Google Earth Engine: Planetary-scale geospatial analysis for everyone, Remote Sens. Environ., 202, 18–27, https://doi.org/10.1016/j.rse.2017.06.031, 2017.

Gray, J. and Song, C.: Consistent classification of image time series with automatic adaptive signature generalization, Remote Sens. Environ., 134, 333–341, https://doi.org/10.1016/j.rse.2013.03.022, 2013.

Hakkenberg, C. R., Dannenberg, M. P., Song, C., and Vinci, G.: Automated Continuous Fields Prediction From Landsat Time Series: Application to Fractional Impervious Cover, IEEE Geosci. Remote Sens. Lett., 17, 132–136, https://doi.org/10.1109/LGRS.2019.2915320, 2020.

Harsch, M. A., Hulme, P. E., McGlone, M. S., and Duncan, R. P.: Are treelines advancing? A global meta-analysis of treeline response to climate warming, Ecol. Lett., 12, 1040–1049, https://doi.org/10.1111/j.1461-0248.2009.01355.x, 2009.

Hermosilla, T., Wulder, M. A., White, J. C., and Coops, N. C.: Land cover classification in an era of big and open data: Optimizing localized implementation and training data selection to improve mapping outcomes, Remote Sens. Environ., 268, 112780, https://doi.org/10.1016/j.rse.2021.112780, 2022.

Hjort, J., Karjalainen, O., Aalto, J., Westermann, S., Romanovsky, V. E., Nelson, F. E., Etzelmüller, B., and Luoto, M.: Degrading permafrost puts Arctic infrastructure at risk by mid-century, Nat. Commun., 9, 5147, https://doi.org/10.1038/s41467-018-07557-4, 2018.

Hodkinson, I. D., Webb, N. R., Bale, J. S., Block, W., Coulson, S. J., and Strathdee, A. T.: Global Change and Arctic Ecosystems: Conclusions and Predictions from Experiments with Terrestrial Invertebrates on Spitsbergen, Arct. Alp. Res., 30, 306–313, https://doi.org/10.1080/00040851.1998.12002904, 1998.

Horvath, P., Tang, H., Halvorsen, R., Stordal, F., Tallaksen, L. M., Berntsen, T. K., and Bryn, A.: Improving the representation of high-latitude vegetation distribution in dynamic global vegetation models, Biogeosciences, 18, 95–112, https://doi.org/10.5194/bg-18-95-2021, 2021.

Huang, H., Wang, J., Liu, C., Liang, L., Li, C., and Gong, P.: The migration of training samples towards dynamic global land cover mapping, ISPRS J. Photogramm. Remote Sens., 161, 27–36, https://doi.org/10.1016/j.isprsjprs.2020.01.010, 2020.

Huang, X., Yang, J., Wang, W., and Liu, Z.: Mapping 10-m global impervious surface area (GISA-10m) using multi-source geospatial data, Earth Syst. Sci. Data Discuss., 2022, 1–39, https://doi.org/10.5194/essd-2021-458, 2022.

Huntington, H. P., Carey, M., Apok, C., Forbes, B. C., Fox, S., Holm, L. K., Ivanova, A., Jaypoody, J., Noongwook, G., and Stammler, F.: Climate change in context: putting people first in the Arctic, Reg. Environ. Change, 19, 1217–1223, https://doi.org/10.1007/s10113-019-01478-8, 2019.

Ingeman-Nielsen, T. and Vakulenko, I.: Calibration and validation data for infrastructure mapping, Greenland, link to files, https://doi.org/10.1594/PANGAEA.895949, 2018.

https://doi.org/10.5194/essd-2022-224
Preprint. Discussion started: 8 August 2022

Jeong, S.-J., Bloom, A. A., Schimel, D., Sweeney, C., Parazoo, N. C., Medvigy, D., Schaepman-Strub, G., Zheng, C., Schwalm, C. R., Huntzinger, D. N., Michalak, A. M., and Miller, C. E.: Accelerating rates of Arctic carbon cycling revealed by long-term atmospheric CO_2 measurements, Sci. Adv., 4, eaao1167, https://doi.org/10.1126/sciadv.aao1167, 2018.

Jia, G. J., Epstein, H. E., and Walker, D. A.: Greening of arctic Alaska, 1981–2001, Geophys. Res. Lett., 30, https://doi.org/10.1029/2003GL018268, 2003.

Jin, S., Yang, L., Zhu, Z., and Homer, C.: A land cover change detection and classification protocol for updating Alaska NLCD 2001 to 2011, Remote Sens. Environ., 195, 44–55, https://doi.org/10.1016/j.rse.2017.04.021, 2017.

Karra, K., Kontgis, C., Statman-Weil, Z., Mazzariello, J. C., Mathis, M., and Brumby, S. P.: Global land use / land cover with Sentinel 2 and deep learning, in: 2021 IEEE International Geoscience and Remote Sensing Symposium IGARSS, 4704–4707, https://doi.org/10.1109/IGARSS47720.2021.9553499, 2021.

Keenan, T. F. and Riley, W. J.: Greening of the land surface in the world's cold regions consistent with recent warming, Nat. Clim. Change, 8, 825–828, https://doi.org/10.1038/s41558-018-0258-y, 2018.

Kohonen, T.: Essentials of the self-organizing map, Neural Netw., 37, 52–65, https://doi.org/10.1016/j.neunet.2012.09.018, 2013.

Kumpula, T., Pajunen, A., Kaarlejärvi, E., Forbes, B. C., and Stammler, F.: Land use and land cover change in Arctic Russia: Ecological and social implications of industrial development, Spec. Issue Polit. Policy Carbon Capture Storage, 21, 550–562, https://doi.org/10.1016/j.gloenvcha.2010.12.010, 2011.

Landrum, L. and Holland, M. M.: Extremes become routine in an emerging new Arctic, Nat. Clim. Change, 10, 1108–1115, https://doi.org/10.1038/s41558-020-0892-z, 2020.

Lang, N., Jetz, W., Schindler, K., and Wegner, J. D.: A high-resolution canopy height model of the Earth, https://doi.org/10.48550/ARXIV.2204.08322, 2022.

Li, C., Gong, P., Wang, J., Zhu, Z., Biging, G. S., Yuan, C., Hu, T., Zhang, H., Wang, Q., Li, X., Liu, X., Xu, Y., Guo, J., Liu, C., Hackman, K. O., Zhang, M., Cheng, Y., Yu, L., Yang, J., Huang, H., and Clinton, N.: The first all-season sample set for mapping global land cover with Landsat-8 data, Sci. Bull., 62, 508–515, https://doi.org/10.1016/j.scib.2017.03.011, 2017.

Li, X. and Gong, P.: An "exclusion-inclusion" framework for extracting human settlements in rapidly developing regions of China from Landsat images, Remote Sens. Environ., 186, 286–296, https://doi.org/10.1016/j.rse.2016.08.029, 2016.

Li, X., Zhou, Y., Meng, L., Asrar, G. R., Lu, C., and Wu, Q.: A dataset of 30 m annual vegetation phenology indicators (1985–2015) in urban areas of the conterminous United States, Earth Syst. Sci. Data, 11, 881–894, https://doi.org/10.5194/essd-11-881-2019, 2019.

Liang, L., Liu, Q., Liu, G., Li, H., and Huang, C.: Accuracy Evaluation and Consistency Analysis of Four Global Land Cover Products in the Arctic Region, Remote Sens., 11, https://doi.org/10.3390/rs11121396, 2019.

Liu, C., Xiong, T., Gong, P., and Qi, S.: Improving large-scale moso bamboo mapping based on dense Landsat time series and auxiliary data: a case study in Fujian Province, China, Remote Sens. Lett., 9, 1–10, https://doi.org/10.1080/2150704X.2017.1378454, 2018.

Liu, C., Zhang, Q., Luo, H., Qi, S., Tao, S., Xu, H., and Yao, Y.: An efficient approach to capture continuous impervious surface dynamics using spatial-temporal rules and dense Landsat time series stacks, Remote Sens. Environ., 229, 114–132, https://doi.org/10.1016/j.rse.2019.04.025, 2019.

Liu, C., Zhang, Q., Tao, S., Qi, J., Ding, M., Guan, Q., Wu, B., Zhang, M., Nabil, M., Tian, F., Zeng, H., Zhang, N., Bavuudorj, G., Rukundo, E., Liu, W., Bofana, J., Beyene, A. N., and Elnashar, A.: A new framework to map fine resolution cropping intensity across the globe: Algorithm, validation, and implication, Remote Sens. Environ., 251, 112095, https://doi.org/10.1016/j.rse.2020.112095, 2020a.

Liu, H., Gong, P., Wang, J., Clinton, N., Bai, Y., and Liang, S.: Annual dynamics of global land cover and its long-term changes from 1982 to 2015, Earth Syst. Sci. Data, 12, 1217–1243, https://doi.org/10.5194/essd-12-1217-2020, 2020b.

Liu, C., Huang, H., Hui, F., Zhang, Z., and Cheng, X.: Fine-Resolution Mapping of Pan-Arctic Lake Ice-Off Phenology Based on Dense Sentinel-2 Time Series Data, Remote Sens., 13, https://doi.org/10.3390/rs13142742, 2021a.

Liu, C., Huang, H., Hui, F., Zhang, Z., and Cheng, X.: Fine-Resolution Mapping of Pan-Arctic Lake Ice-Off Phenology Based on Dense Sentinel-2 Time Series Data, Remote Sens., 13, https://doi.org/10.3390/rs13142742, 2021b.

Liu, H., Gong, P., Wang, J., Wang, X., Ning, G., and Xu, B.: Production of global daily seamless data cubes and quantification of global land cover change from 1985 to 2020 - iMap World 1.0, Remote Sens. Environ., 258, 112364, https://doi.org/10.1016/j.rse.2021.112364, 2021c.

Liu, C., Huang, H., Zhang, Q., Chen, X., Xu, X., Xu, H., and Cheng, X.: Arctic's man-made impervious surfaces expanded by over two-thirds in the 21st century, Sci. Bull., https://doi.org/10.1016/j.scib.2022.06.001, 2022.

Loveland, T. R. and Belward, A. S.: The International Geosphere Biosphere Programme Data and Information System global land cover data set (DISCover), Acta Astronaut., 41, 681–689, https://doi.org/10.1016/S0094-5765(98)00050-2, 1997.

Loveland, T. R., Reed, B. C., Brown, J. F., Ohlen, D. O., Zhu, Z., Yang, L., and Merchant, J. W.: Development of a global land cover characteristics database and IGBP DISCover from 1 km AVHRR data, Int. J. Remote Sens., 21, 1303–1330, https://doi.org/10.1080/014311600210191, 2000.

Lu, W., Aalberg, A., Høyland, K. V., Lubbad, R., Løset, S., and Ingeman-Nielsen, T.: Calibration data for Infrastructure mapping in Svalbard, link to files, https://doi.org/10.1594/PANGAEA.895950, 2018.

Magnússon, R. Í., Limpens, J., Kleijn, D., Huissteden, K. van, Maximov, T. C., Lobry, S., and Heijmans, M. M. P. D.: Shrub decline and expansion of wetland vegetation revealed by very high resolution land cover change detection in the Siberian lowland tundra, Sci. Total Environ., 782, 146877, https://doi.org/10.1016/j.scitotenv.2021.146877, 2021.

Miner, K. R., Turetsky, M. R., Malina, E., Bartsch, A., Tamminen, J., McGuire, A. D., Fix, A., Sweeney, C., Elder, C. D., and Miller, C. E.: Permafrost carbon emissions in a changing Arctic, Nat. Rev. Earth Environ., 3, 55–67, https://doi.org/10.1038/s43017-021-00230-3, 2022.

Moon, T. A., Overeem, I., Druckenmiller, M., Holland, M., Huntington, H., Kling, G., Lovecraft, A. L., Miller, G., Scambos, T., Schädel, C., Schuur, E. A. G., Trochim, E., Wiese, F., Williams, D., and Wong, G.: The Expanding Footprint of Rapid Arctic Change, Earths Future, 7, 212–218, https://doi.org/10.1029/2018EF001088, 2019.

Myers-Smith, I. H., Kerby, J. T., Phoenix, G. K., Bjerke, J. W., Epstein, H. E., Assmann, J. J., John, C., Andreu-Hayles, L., Angers-Blondin, S., Beck, P. S. A., Berner, L. T., Bhatt, U. S., Bjorkman, A. D., Blok, D., Bryn, A., Christiansen, C. T., Cornelissen, J. H. C., Cunliffe, A. M., Elmendorf, S. C., Forbes, B. C., Goetz, S. J., Hollister, R. D., de Jong, R., Loranty, M.

https://doi.org/10.5194/essd-2022-224
Preprint. Discussion started: 8 August 2022

M., Macias-Fauria, M., Maseyk, K., Normand, S., Olofsson, J., Parker, T. C., Parmentier, F.-J. W., Post, E., Schaepman-Strub, G., Stordal, F., Sullivan, P. F., Thomas, H. J. D., Tømmervik, H., Treharne, R., Tweedie, C. E., Walker, D. A., Wilmking, M., and Wipf, S.: Complexity revealed in the greening of the Arctic, Nat. Clim. Change, 10, 106–117, https://doi.org/10.1038/s41558-019-0688-1, 2020.

Najafi, M. R., Zwiers, F. W., and Gillett, N. P.: Attribution of Arctic temperature change to greenhouse-gas and aerosol influences, Nat. Clim. Change, 5, 246–249, https://doi.org/10.1038/nclimate2524, 2015.

Niittynen, P., Heikkinen, R. K., and Luoto, M.: Snow cover is a neglected driver of Arctic biodiversity loss, Nat. Clim. Change, 8, 997–1001, https://doi.org/10.1038/s41558-018-0311-x, 2018.

Pastorello, G., Trotta, C., Canfora, E., Chu, H., Christianson, D., Cheah, Y.-W., Poindexter, C., Chen, J., Elbashandy, A., Humphrey, M., Isaac, P., Polidori, D., Ribeca, A., van Ingen, C., Zhang, L., Amiro, B., Ammann, C., Arain, M. A., Ardö, J., Arkebauer, T., Arndt, S. K., Arriga, N., Aubinet, M., Aurela, M., Baldocchi, D., Barr, A., Beamesderfer, E., Marchesini, L. B., Bergeron, O., Beringer, J., Bernhofer, C., Berveiller, D., Billesbach, D., Black, T. A., Blanken, P. D., Bohrer, G., Boike, J., Bolstad, P. V., Bonal, D., Bonnefond, J.-M., Bowling, D. R., Bracho, R., Brodeur, J., Brümmer, C., Buchmann, N., Burban, B., Burns, S. P., Buysse, P., Cale, P., Cavagna, M., Cellier, P., Chen, S., Chini, I., Christensen, T. R., Cleverly, J., Collalti, A., Consalvo, C., Cook, B. D., Cook, D., Coursolle, C., Cremonese, E., Curtis, P. S., D'Andrea, E., da Rocha, H., Dai, X., Davis, K. J., De Cinti, B., de Grandcourt, A., De Ligne, A., De Oliveira, R. C., Delpierre, N., Desai, A. R., Di Bella, C. M., di Tommasi, P., Dolman, H., Domingo, F., Dong, G., Dore, S., Duce, P., Dufrêne, E., Dunn, A., Dušek, J., Eamus, D., Eichelmann, U., ElKhidir, H. A. M., Eugster, W., Ewenz, C. M., Ewers, B., Famulari, D., Fares, S., Feigenwinter, I., Feitz, A., Fensholt, R., Filippa, G., Fischer, M., Frank, J., Galvagno, M., Gharun, M., Gianelle, D., et al.: The FLUXNET2015 dataset and the ONEFlux processing pipeline for eddy covariance data, Sci. Data, 7, 225, https://doi.org/10.1038/s41597-020-0534-3, 2020.

Porter, C., Morin, P., Howat, I., Noh, M.-J., Bates, B., Peterman, K., Keesey, S., Schlenk, M., Gardiner, J., Tomko, K., Willis, M., Kelleher, C., Cloutier, M., Husby, E., Foga, S., Nakamura, H., Platson, M., Wethington, M., Jr., Williamson, C., Bauer, G., Enos, J., Arnold, G., Kramer, W., Becker, P., Doshi, A., D'Souza, C., Cummens, P., Laurier, F., and Bojesen, M.: ArcticDEM, , https://doi.org/10.7910/DVN/OHHUKH, 2018.

Potapov, P., Turubanova, S., Hansen, M. C., Tyukavina, A., Zalles, V., Khan, A., Song, X.-P., Pickens, A., Shen, Q., and Cortez, J.: Global maps of cropland extent and change show accelerated cropland expansion in the twenty-first century, Nat. Food, 3, 19–28, https://doi.org/10.1038/s43016-021-00429-z, 2022.

Previdi, M., Smith, K. L., and Polvani, L. M.: Arctic amplification of climate change: a review of underlying mechanisms, Environ. Res. Lett., 16, 093003, https://doi.org/10.1088/1748-9326/ac1c29, 2021.

Raynolds, M. K., Walker, D. A., Ambrosius, K. J., Brown, J., Everett, K. R., Kanevskiy, M., Kofinas, G. P., Romanovsky, V. E., Shur, Y., and Webber, P. J.: Cumulative geoecological effects of 62 years of infrastructure and climate change in ice-rich permafrost landscapes, Prudhoe Bay Oilfield, Alaska, Glob. Change Biol., 20, 1211–1224, https://doi.org/10.1111/gcb.12500, 2014.

Raynolds, M. K., Walker, D. A., Balser, A., Bay, C., Campbell, M., Cherosov, M. M., Daniëls, F. J. A., Eidesen, P. B., Ermokhina, K. A., Frost, G. V., Jedrzejek, B., Jorgenson, M. T., Kennedy, B. E., Kholod, S. S., Lavrinenko, I. A., Lavrinenko, O. V., Magnússon, B., Matveyeva, N. V., Metúsalemsson, S., Nilsen, L., Olthof, I., Pospelov, I. N., Pospelova, E. B., Pouliot, D., Razzhivin, V., Schaepman-Strub, G., Šibík, J., Telyatnikov, M. Yu., and Troeva, E.: A raster version of the Circumpolar Arctic Vegetation Map (CAVM), Remote Sens. Environ., 232, 111297, https://doi.org/10.1016/j.rse.2019.111297, 2019.

Rees, W. G., Hofgaard, A., Boudreau, S., Cairns, D. M., Harper, K., Mamet, S., Mathisen, I., Swirad, Z., and Tutubalina, O.: Is subarctic forest advance able to keep pace with climate change?, Glob. Change Biol., 26, 3965–3977, https://doi.org/10.1111/gcb.15113, 2020.

Richardson, A. D., Hufkens, K., Milliman, T., Aubrecht, D. M., Chen, M., Gray, J. M., Johnston, M. R., Keenan, T. F., Klosterman, S. T., Kosmala, M., Melaas, E. K., Friedl, M. A., and Frolking, S.: Tracking vegetation phenology across diverse North American biomes using PhenoCam imagery, Sci. Data, 5, 180028, https://doi.org/10.1038/sdata.2018.28, 2018.

Shepherd, A., Ivins, E., Rignot, E., Smith, B., van den Broeke, M., Velicogna, I., Whitehouse, P., Briggs, K., Joughin, I., Krinner, G., Nowicki, S., Payne, T., Scambos, T., Schlegel, N., A, G., Agosta, C., Ahlstrøm, A., Babonis, G., Barletta, V. R., Bjørk, A. A., Blazquez, A., Bonin, J., Colgan, W., Csatho, B., Cullather, R., Engdahl, M. E., Felikson, D., Fettweis, X., Forsberg, R., Hogg, A. E., Gallee, H., Gardner, A., Gilbert, L., Gourmelen, N., Groh, A., Gunter, B., Hanna, E., Harig, C., Helm, V., Horvath, A., Horwath, M., Khan, S., Kjeldsen, K. K., Konrad, H., Langen, P. L., Lecavalier, B., Loomis, B., Luthcke, S., McMillan, M., Melini, D., Mernild, S., Mohajerani, Y., Moore, P., Mottram, R., Mouginot, J., Moyano, G., Muir, A., Nagler, T., Nield, G., Nilsson, J., Noël, B., Otosaka, I., Pattle, M. E., Peltier, W. R., Pie, N., Rietbroek, R., Rott, H., Sandberg Sørensen, L., Sasgen, I., Save, H., Scheuchl, B., Schrama, E., Schröder, L., Seo, K.-W., Simonsen, S. B., Slater, T., Spada, G., Sutterley, T., Talpe, M., Tarasov, L., van de Berg, W. J., van der Wal, W., van Wessem, M., Vishwakarma, B. D., Wiese, D., Wilton, D., Wagner, T., Wouters, B., Wuite, J., and The IMBIE Team: Mass balance of the Greenland Ice Sheet from 1992 to 2018, Nature, 579, 233–239, https://doi.org/10.1038/s41586-019-1855-2, 2020.

Shevtsova, I., Heim, B., Kruse, S., Schroeder, J., Troeva, E., Pestryakova, L. A., Zakharov, E. S., and Herzschuh, U.: Strong shrub expansion in tundra-taiga, tree infilling in taiga and stable tundra in central Chukotka (north-eastern Siberia) between 2000 and 2017, Environ. Res. Lett., 15, 085006, https://doi.org/10.1088/1748-9326/ab9059, 2020.

Song, X.-P., Hansen, M. C., Stehman, S. V., Potapov, P. V., Tyukavina, A., Vermote, E. F., and Townshend, J. R.: Global land change from 1982 to 2016, Nature, 560, 639–643, https://doi.org/10.1038/s41586-018-0411-9, 2018.

Walker, D. A., Raynolds, M. K., Daniëls, F. J. A., Einarsson, E., Elvebakk, A., Gould, W. A., Katenin, A. E., Kholod, S. S., Markon, C. J., Melnikov, E. S., Moskalenko, N. G., Talbot, S. S., Yurtsev, B. A. (†), and Team, T. other members of the C.: The Circumpolar Arctic vegetation map, J. Veg. Sci., 16, 267–282, https://doi.org/10.1111/j.1654-1103.2005.tb02365.x, 2005.

Wang, J. A. and Friedl, M. A.: The role of land cover change in Arctic-Boreal greening and browning trends, Environ. Res. Lett., 14, 125007, https://doi.org/10.1088/1748-9326/ab5429, 2019.

Wang, J. A., Sulla-Menashe, D., Woodcock, C. E., Sonnentag, O., Keeling, R. F., and Friedl, M. A.: Extensive land cover change across Arctic–Boreal Northwestern North America from disturbance and climate forcing, Glob. Change Biol., 26, 807–822, https://doi.org/10.1111/gcb.14804, 2020.

Wulder, M. A., Coops, N. C., Roy, D. P., White, J. C., and Hermosilla, T.: Land cover 2.0, Int. J. Remote Sens., 39, 4254–4284, https://doi.org/10.1080/01431161.2018.1452075, 2018.

Xu, X., Liu, C., Liu, C., Hui, F., Cheng, X., and Huang, H.: Circumpolar Arctic Land Cover for circa 2020 (CALC-2020), , https://doi.org/10.57760/sciencedb.01869, 2022a.

Xu, X., Liu, C., Liu, C., Hui, F., Cheng, X., and Huang, H.: Fine-resolution mapping of the circumpolar Arctic Man-made impervious areas (CAMI) using sentinels, OpenStreetMap and ArcticDEM, Big Earth Data, 0, 1–22, https://doi.org/10.1080/20964471.2022.2025663, 2022b.

Yu, Q., Epstein, H. E., Engstrom, R., Shiklomanov, N., and Strelestskiy, D.: Land cover and land use changes in the oil and gas regions of Northwestern Siberia under changing climatic conditions, Environ. Res. Lett., 10, 124020, https://doi.org/10.1088/1748-9326/10/12/124020, 2015.

https://doi.org/10.5194/essd-2022-224
Preprint. Discussion started: 8 August 2022

Zanaga, D., Van De Kerchove, R., De Keersmaecker, W., Souverijns, N., Brockmann, C., Quast, R., Wevers, J., Grosu, A., Paccini, A., Vergnaud, S., Cartus, O., Santoro, M., Fritz, S., Georgieva, I., Lesiv, M., Carter, S., Herold, M., Li, L., Tsendbazar, N.-E., Ramoino, F., and Arino, O.: ESA WorldCover 10 m 2020 v100, 2020.

Zhang, X., Liu, L., Wu, C., Chen, X., Gao, Y., Xie, S., and Zhang, B.: Development of a global 30\,m impervious surface map using multisource and multitemporal remote sensing datasets with the Google Earth Engine platform, Earth Syst. Sci. Data, 12, 1625–1648, https://doi.org/10.5194/essd-12-1625-2020, 2020.

Zhang, X., Liu, L., Chen, X., Gao, Y., Xie, S., and Mi, J.: GLC_FCS30: global land-cover product with fine classification system at 30\,m using time-series Landsat imagery, Earth Syst. Sci. Data, 13, 2753–2776, https://doi.org/10.5194/essd-13-2753-2021, 2021a.

Zhang, Y., Song, C., Hwang, T., Novick, K., Coulston, J. W., Vose, J., Dannenberg, M. P., Hakkenberg, C. R., Mao, J., and Woodcock, C. E.: Land cover change-induced decline in terrestrial gross primary production over the conterminous United States from 2001 to 2016, Agric. For. Meteorol., 308–309, 108609, https://doi.org/10.1016/j.agrformet.2021.108609, 2021b.

Zhu, Z., Woodcock, C. E., Rogan, J., and Kellndorfer, J.: Assessment of spectral, polarimetric, temporal, and spatial dimensions for urban and peri-urban land cover classification using Landsat and SAR data, Remote Sens. Environ., 117, 72–82, https://doi.org/10.1016/j.rse.2011.07.020, 2012.

Zhu, Z., Gallant, A. L., Woodcock, C. E., Pengra, B., Olofsson, P., Loveland, T. R., Jin, S., Dahal, D., Yang, L., and Auch, R. F.: Optimizing selection of training and auxiliary data for operational land cover classification for the LCMAP initiative, ISPRS J. Photogramm. Remote Sens., 122, 206–221, https://doi.org/10.1016/j.isprsjprs.2016.11.004, 2016.